Journal of Medicinal Chemistry

Fluorescent-labeled selective adenosine A2B receptor antagonist enables competition binding assay by flow cytometry

Meryem Köse, Sabrina Gollos, Tadeusz Karcz, Amelie Fiene, Fabian Heisig, Andrea Behrenswerth, Katarzyna J. Kiec-Kononowicz, Vigneshwaran Namasivayam, and Christa E Müller

J. Med. Chem., **Just Accepted Manuscript** • DOI: 10.1021/acs.jmedchem.7b01627 • Publication Date (Web): 22 Apr 2018

ACS Publications

is published by the American Chemical Society. 1155 Sixteenth Street N.W., Washington, DC 20036

Fluorescent-labeled selective adenosine A_{2B} receptor antagonist enables competition binding assay by flow cytometry

Meryem Köse,[1≠] Sabrina Gollos,[1≠] Tadeusz Karcz,[2] Amelie Fiene,[1] Fabian Heisig,[1] Andrea Behrenswerth,[1] Katarzyna Kieć-Kononowicz,[2] Vigneshwaran Namasivayam,[1] and Christa E. Müller[1]**

[1]PharmaCenter Bonn, Pharmaceutical Institute, Pharmaceutical Chemistry I, University of Bonn, An der Immenburg 4, D-53121 Bonn, Germany, [2]Department of Technology and Biotechnology of Drugs, Faculty of Pharmacy, Jagiellonian University Medical College, Medyczna 9, 30-688, Kraków, Poland

[≠]authors contributed equally

KEYWORDS: GPCR, adenosine A_{2B} receptor, antagonist, BODIPY, fluorescent ligand, fluorophore, synthesis

ABSTRACT

Fluorescent ligands represent powerful tools for biological studies and are considered as attractive alternatives to radioligands. In this study, we developed fluorescent antagonists for A_{2B} adenosine receptors (A_{2B}ARs), which are targeted by anti-asthmatic xanthines and were proposed as novel targets in immuno-oncology. Our approach was to merge a small borondipyrromethene (BODIPY) derivative with the pharmacophore of 8-substituted xanthine derivatives. Based on the design, synthesis and evaluation of model compounds several fluorescent ligands were synthesized. Compound **29** (PSB-12105), which displays high affinity for human, rat and mouse A_{2B}ARs (K_i 0.2-2 nM) and high selectivity versus all other AR subtypes, was selected for further studies. A homology model of the human A_{2B}AR was generated and docking studies were performed. Moreover, **29** served to establish a homogeneous receptor-ligand binding assay using flow cytometry. These compounds constitute the first potent, selective fluorescent A_{2B}AR ligands and are anticipated to be useful for a variety of applications.

INTRODUCTION

Adenosine acts as a signaling molecule by activating G protein-coupled membrane receptors (GPCRs) termed A_1, A_{2A}, A_{2B} and A_3 adenosine receptors (ARs).[1] These receptors are ubiquitously expressed, but their expression levels and subtype distribution is organ- and tissue-specific. Moreover, AR expression is regulated under pathological conditions, e.g. upregulation of A_{2B}ARs is observed under inflammatory, ischemic and hypoxic conditions. The specific blockade of the A_{2B}AR subtype has been proposed as a novel strategy, e.g. for the treatment of asthma, inflammatory bowel disease, pain, diabetes, sickle cell disease, and cancer.[2-6] The effectiveness of A_{2B}AR antagonists in preclinical cancer models has recently attracted much attention since they do not only prevent suppression of immune cells by adenosine in the microenvironment of cancer tissues, similarly as A_{2A}AR antagonists, but they additionally display direct anti-proliferative effects on cancer cells and inhibit angiogenesis.[7-9] Moreover, we recently showed that A_{2B}ARs can form homomeric assemblies and heteromeric complexes with the closely related A_{2A}AR subtype. The A_{2B}AR is thereby able to completely block A_{2A}AR signaling.[10]

In drug development the direct measurement of receptor-ligand affinity provides important information. Radioligands are typically used to obtain these data, in particular ^{3}H- or ^{131}I-labeled compounds that are used for in vitro studies, while ^{18}F- or ^{11}C-labeled tracers are suitable for in vivo studies employing positron emission tomography (PET). Due to the high costs of radioligands, the risk in handling radioactive materials, and the problem of producing radioactive waste with a long half-life of more than 12 years in case of the frequently employed ^{3}H-labeled ligands, the development of fluorescent ligands has gained importance and may become the future method of choice, especially for in vitro studies. Fluorescent ligands enable the

application of powerful techniques including fluorescence polarization (FP),[11] fluorescence correlation spectroscopy (FCS),[12-14] fluorescence resonance energy transfer (FRET),[15,16] flow cytometry[17] and fluorescence recovery after photobleaching (FRAP) experiments.[18] Several fluorescent-labeled ligands for ARs, agonists and antagonists, have already been described[11-17, 19-37] and some of them were shown to be useful tools for studying the receptors on a molecular level [38,39]. Fluorescent-labeled adenosine and *N*-ethylcarboxamidoadenosine (NECA) derivatives were prepared by attaching fluorophores via long linkers to the adenine N^6- or C2-position (see compounds **1-9**, Figure 1). However, most of the obtained fluorescent agonists also activate A_1-, A_{2A}- and A_3ARs and are thus non-selective.[12-14, 21-24, 31-32, 34, 40-42] Selective fluorescent A_3AR agonists were developed by coupling of a potent and selective A_3 agonist (MRS3558) with the fluorophores Cy5 (**7**, MRS5218)[26], squaraine-rotaxane (**8**, MRS5243)[27], or 4-pyrene (**9**, MRS5704)[29] (for structures see Figure 1). The determined affinities at the human A_3AR were in the nanomolar range (17.2 nM, 239 nM and 68.3 nM, respectively).

Fluorescent AR antagonists have also been prepared (see, for examples, compounds **10-12** in Figure 2. These were based on the xanthine derivative 8-[4-[[[[(2-aminoethyl)amino]carbonyl]methyl]oxy]phenyl]-l,3-dipropylxanthine (XAC), e.g. compound **10**, the pyrazolotriazolopyrimidine derivative 2-(2-furanyl)-7-[3-(4-methoxyphenyl)propyl]-7*H*-pyrazolo[4,3-*e*][1,2,4]triazolo[1,5-*c*]pyrimidin-5-amine (SCH442416), or the related triazoloquinazoline derivative 9-chloro-2-(2-furyl)[1,2,4]triazolo[1,5-*c*]quinazolin-5-amine (CGS15943), e.g. compounds **11** and **12**, to which fluorescent dyes were attached.[11,13,17,33,37] Compound **11** (MRS5449) was found to be a potent A_3AR antagonist (K_i 6.4 nM, human A_3AR) but displayed low selectivity versus the other AR subtypes (K_i 73.0 nM at the human A_{2A}AR, 87.0 nM at the human A_1AR)[17] (see Figure 2). Moreover, fluorescent-labeled dendrimers were

developed as ligands for A_1-, A_{2A}- or A_3ARs.[25,27] Recently, the first fluorescence-based binding assays for ARs – specifically for the A_3AR subtype – were developed.[17,39] So far, no A_{2B}-selective fluorescent AR ligands have been reported.

Typically used fluorophores include fluorescein, rhodamine, coumarine and borondipyrromethene (BODIPY) derivatives[43]. Traditional fluorophores such as dansyl, pyrene and FITC are fraught with significant drawbacks including pH sensitivity and short fluorophore excitation wavelength interfering with autofluorescence of cells and tissues, which hinders their use as molecular probes. BODIPY derivatives display a number of advantages, e.g. they are photochemically stable, show high absorption coefficients and high fluorescence quantum yields resulting high peak intensity. Moreover, they display λ_{max} values of $\geq$ 500 up to 630 nm depending on the substitution pattern. All of these properties make them ideally suitable fluorophores for biological studies.[44-47] We previously reported on the synthesis of small BODIPY derivatives bearing a variety of functional groups, which can readily be coupled to target molecules. Moreover, we had demonstrated their utility by synthesizing a fluorescent-labeled A_3AR agonist.[48]

In the present study, we designed and developed the first fluorescent A_{2B}AR ligands by integrating a BODIPY into the pharmacophore of an A_{2B}-selective AR antagonist. This led to compounds with high affinity and A_{2B}AR subtype-selectivity. Moreover, we applied one of the new fluorescent A_{2B}AR ligands for establishing a flow cytometry-based A_{2B}AR fluorescence binding assays, which is performed on living cells and may be used to replace radioligand binding studies.

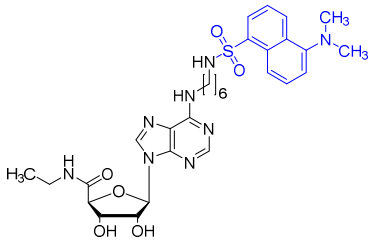

1
Dansyl-labeled NECA derivative[22]
K_i (rat A_1AR): 27 nM
K_i (rat A_{2A}): 4,600 nM
K_i (rat A_3): 3,600 nM

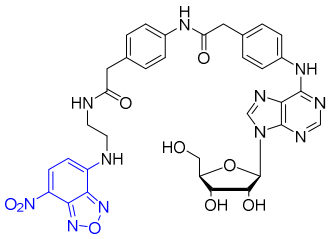

2
7-Nitrobenzofurazan-4-yl- (NBD-) labeled adenosine derivative[33]
K_i (rat A_1): 4.3 nM

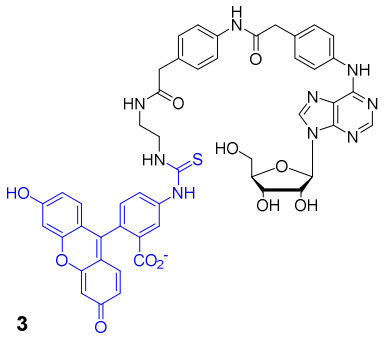

3
Fluorescein isothiocyanate- (FITC-) labeled adenosine derivative[33]
K_i (rat A_1): 7.1 nM

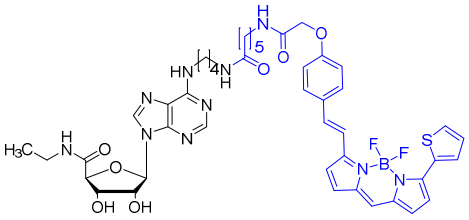

4
BODIPY 630/650-X-labeled NECA derivative[12]
EC_{50} (cAMP, human A_1): 3.39 nM
K_D (human A_1): 158 nM
EC_{50} (cAMP, human A_{2A}): 174 nM
EC_{50} (cAMP, human A_{2B}): 2,04 nM
EC_{50} (cAMP, human A_3): 2.69 nM

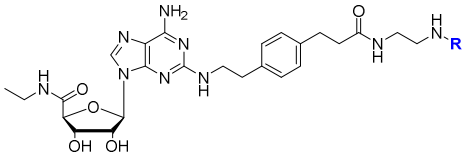

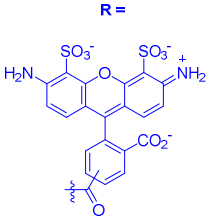

5
Alexa488-labeled NECA derivative[31]
K_i (human A_1): no binding
K_i (human A_{2A}): 149 nM
K_i (human A_3): 240 nM

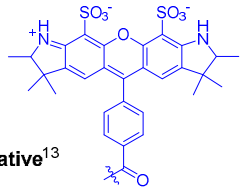

6 (MRS5424)
Alexa Fluor-532-labeled NECA derivative[13]

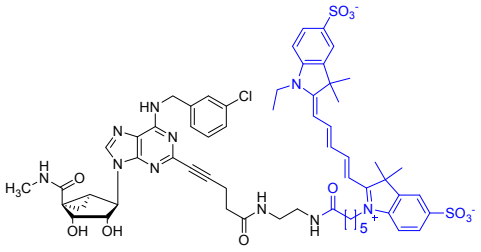

7 (MRS5218)[26]
Cy5-labeled adenosine analog
K_i (human A_1): no binding
K_i (human A_{2A}): 4730 nM
K_i (human A_3): 17.2 nM

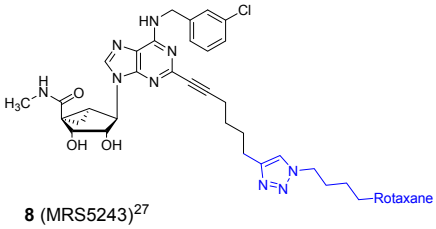

8 (MRS5243)[27]
Squaraine rotaxane-labeled adenosine analog
K_i (human A_1): no binding
K_i (human A_{2A}): no binding
K_i (human A_3): 239 nM

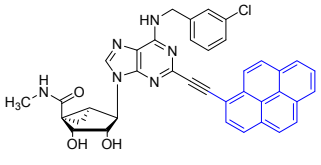

9 (MRS5704)[29]
4-Pyrenyl-labeled adenosine analog
K_i (human A_1): no binding
K_i (human A_{2A}): 3110 nM
K_i (human A_3): 68.3 nM

Figure 1. Examples of fluorescent labeled AR agonists

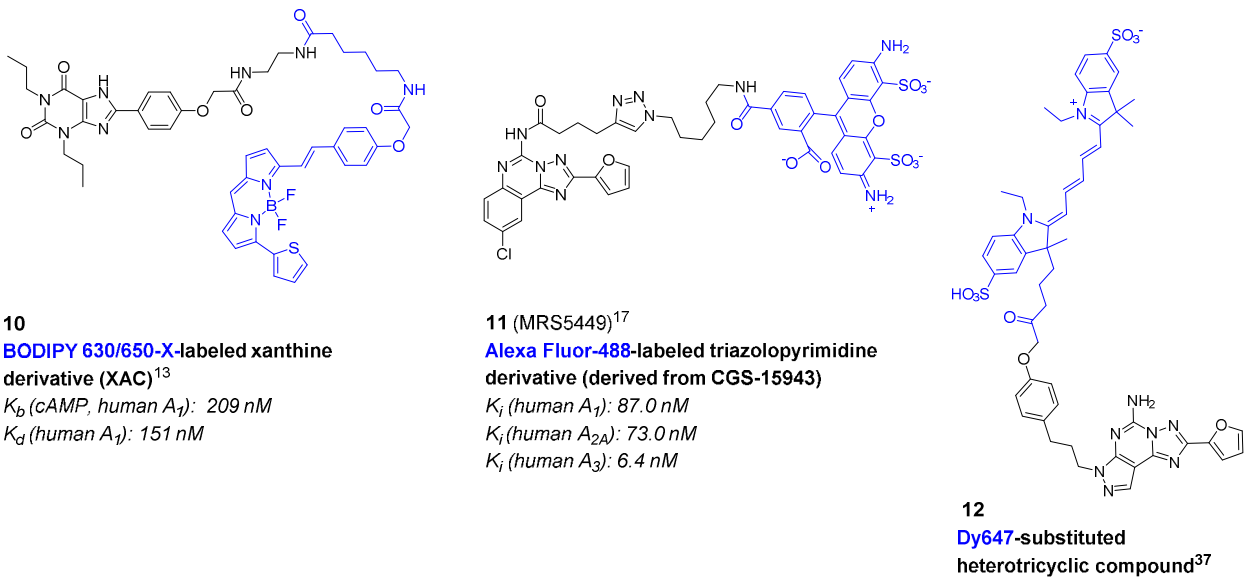

10
BODIPY 630/650-X-labeled xanthine derivative (XAC)[13]
K_b (cAMP, human A_1): 209 nM
K_d (human A_1): 151 nM

11 (MRS5449)[17]
Alexa Fluor-488-labeled triazolopyrimidine derivative (derived from CGS-15943)
K_i (human A_1): 87.0 nM
K_i (human A_{2A}): 73.0 nM
K_i (human A_3): 6.4 nM

12
Dy647-substituted heterotricyclic compound[37]

Figure 2. Structures of selected fluorescent adenosine receptor antagonists

A fluorescent receptor ligand with ideal properties for the desired biological studies would combine the following properties: (i) high wavelength of excitation (> 350 nm) and emission, (ii) water-solubility, (iii) high absorption coefficient and high fluorescence quantum yield resulting in high peak intensity, (iv) small size in order not to interfere with binding to the target, and (v) photochemical stability (under basic, reductive and oxidative conditions).

RESULTS AND DISCUSSION

Design and synthesis of model compounds

Our approach was to design a fluorescent A_{2B}-selective AR antagonist by integrating a small fluorophore into the target structure as part of its pharmacophore. This is different from most previous approaches which utilized the attachment of a mostly large fluorophore via a long linker to the AR ligand (see Figure 1 and 2). We had previously discovered that 3-unsubstituted 8-phenyl-1-propylxanthine derivatives generally displayed higher A_{2B}AR affinity and subtype-selectivity than the corresponding 1,3-substituted derivatives. Based on the known structure-activity relationships for xanthine derivatives,[49] and supported by homology modeling and docking studies[50] (also see molecular modeling studies described below) we designed fluorescent-labeled derivatives in which the fluorophore was to be introduced into the *para*-position of the 8-phenyl ring, at which larger substituents are known to be well tolerated and can even contribute to high affinity and selectivity. A small (carboxymethyl)oxy linkage was selected to connect the fluorophore to the 8-phenyl-1-propylxanthine core structure, which would then allow to introduce an amino-substituted fluorophore by amide formation. We had previously developed a synthetic access to a toolbox of small, functionalized green-emitting BODIPY derivatives, including amino-substituted compounds such as **13**-**17**, which can readily be coupled to target molecules (see Figure 3).[48]

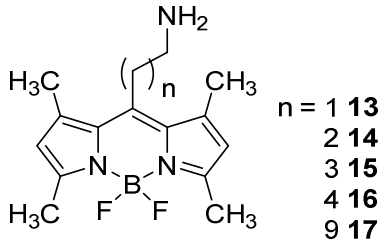

Figure 3. Synthesized amino-functionalized BODIPY derivatives

In order to probe whether lipophilic, aromatic residues like BODIPY derivatives were actually tolerated at that position by the A_{2B}AR, and in particular to investigate the optimal linker length between the xanthine core and the attached ring system,

we initially prepared several model compounds. Instead of the precious BODIPY derivatives we attached a simple phenyl ring. Even a small BODIPY derivative is considerably more lipophilic and larger than a phenyl ring, and therefore, it has to be kept in mind that this constitutes a simplification. Compounds **25-28** were synthesized starting from 6-aminouracil (**18**) via 1-propylpurine-2,6-dione-8-phenoxyacetic acid (**24**) in analogy to published procedures (Scheme 1).[51-54]

Scheme 1. Synthesis of model compounds **25-28** substituted with a phenyl ring instead of a fluorescent BODIPY residue

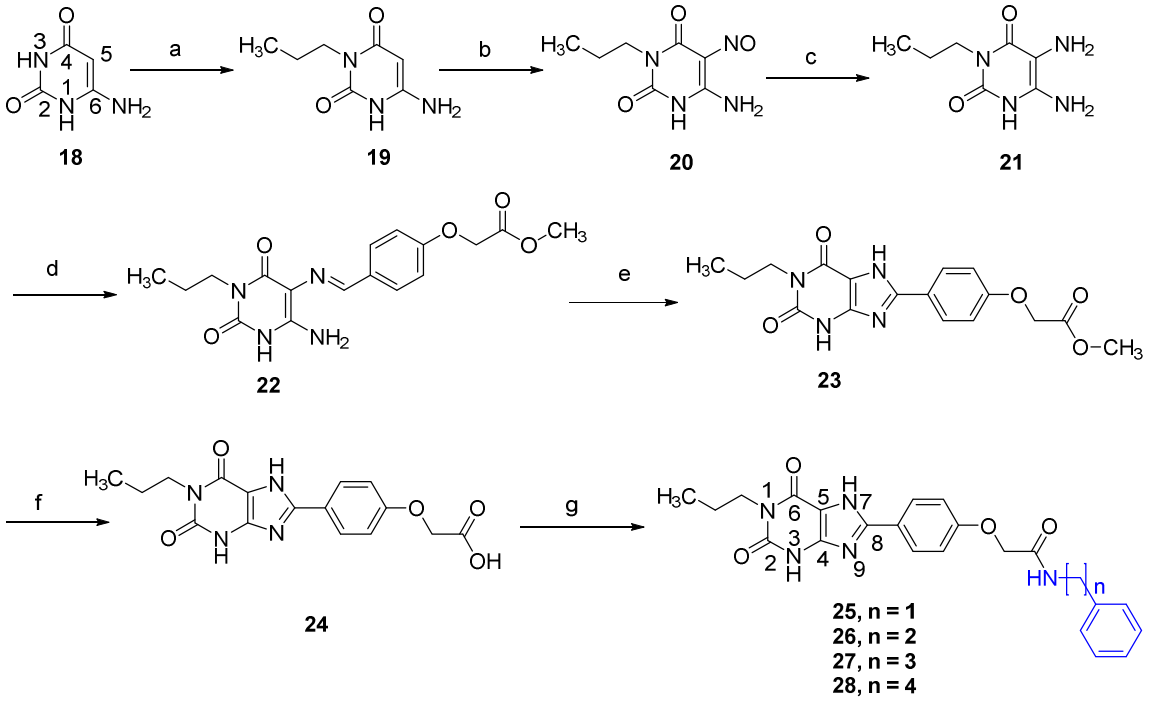

Reaction conditions: [a](i) Hexamethyldisilazane (HMDS), $(NH_4)_2SO_4$, reflux for 2h; (ii) propyl bromide, reflux for 1.5 h; (iii) addition of $Na_2S_2O_3$ in H_2O, followed by saturated aq. $NaHCO_3$ solution at 0°C. [b]Dimethylformamide (DMF)/H_2O, $NaNO_2$, concd. aq. HCl, 70°C, 1 h. [c]Methanol (MeOH), PtO_2/H_2 (42 psi), rt, 2 h. [d]Methyl-(4-formylphenoxy)acetate, ethanol, reflux,

30 min. [e]Thionyl chloride, heating from 0°C to 70 °C, 2 h. [f]DMF, 0.1-*N* aq. Na_2CO_3 solution, 100°C, 30 min. [g]*N*-Methylmorpholine, DMF; addition of isobutyl chloroformate and the appropriate phenylalkylamine at -22°C, warming to rt for 3h.

6-Amino-3-propyluracil (**19**) was obtained in 81 % yield by regioselective alkylation of 6-aminouracil (**18**) with propyl bromide according to a method developed by Müller.[53] Compound **19** was nitrosated with $NaNO_2$/acetic acid (AcOH) and subsequently reduced with H_2/PtO_2 to obtain 5,6-diamino-3-propyluracil (**21**). Since **21** is sensitive to humidity and to oxidation by air it was immediately reacted with methyl-(4-formylphenoxy) acetate yielding **22** in excellent yield (98 %). Ring closure was performed by treatment with thionyl chloride at 70°C yielding xanthine derivative **23**. The methyl ester function was cleaved by heating with base (Na_2CO_3) in DMF/H_2O to obtain the free carboxylic acid **24**. Amide formation of **24** was achieved by the addition of the appropriate phenylalkylamine in the presence of *N*-methylmorpholine and isobutyl chloroformate leading to the desired products **25-28**.

Synthesis of BODIPY-labeled A_{2B}AR antagonists 29-33

Since different linker lengths were tolerated, but structure-activity relationships of the phenyl-substituted model compounds and the BODIPY-substituted analogs appeared to be somewhat different, we decided to prepare a series of BODIPY-labeled xanthine derivatives. The amino-substituted BODIPY derivatives **13-17** were synthesized as previously described[48] and subsequently coupled with xanthine **24** in the presence of 2-(6-chloro-1*H*-benzotriazol-1-yl)-1,1,3,3-tetramethyluronium hexafluorophosphate (HCTU), 1-hydroxybenzotriazole (HOBt) and *N*-methylmorpholine as a base (for **29** and **32**) or by reaction with isobutyl chloroformate in the

presence of *N*-methylmorpholine (for **30**, **31** and **33**) (see Scheme 2). The former method provided somewhat higher yields. The fluorescent ligands **29-33** were purified by flash chromatogaphy on silica gel yielding 11-40 % of pure products (for details see Experimental Section).

Scheme 2. Synthesis of the fluorescent ligands **29-33**

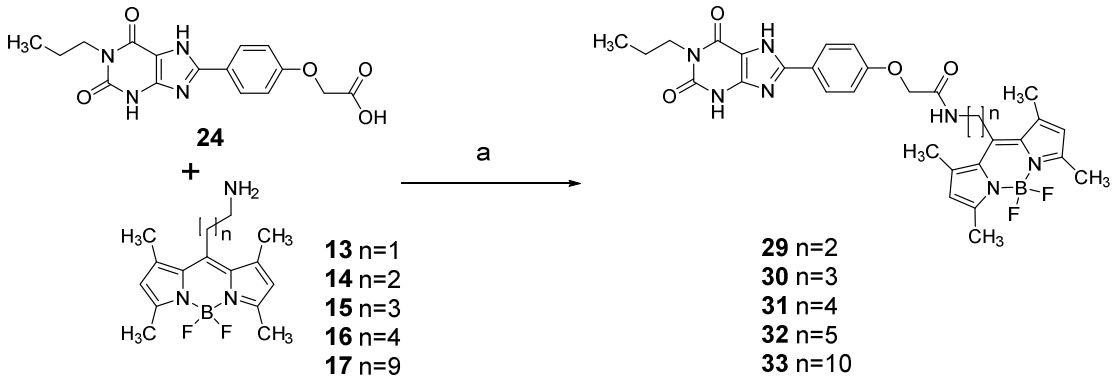

Reaction conditions: [a]HCTU, HOBt, *N*-methylmorpholine, dry DMF, rt, 16h for the preparation of **29** (40% yield) and **32** (30% yield); isobutyl chloroformate, *N*-methylmorpholine, dry DMF, rt 3h, for the synthesis of **30** (22% yield), **31** (17% yield), and **33** (11% yield).

Analysis of the products

All products were analyzed by HPLC-(DAD)UV-(ESI)MS analysis and showed at least 95 % purity. The structures of the new compounds were confirmed by ^{1}H and ^{13}C NMR spectra. The fluorescent properties of **29** were determined by fluorescence spectroscopy. The absorption maximum was at 497 nm, and the emission at 498 nm (for absorption and emission spectra see Figure S1 in Supporting Information). The fluorescence quantum yield was measured in ethanol

with rhodamine 6G as a reference compound and was found to be 0.94, close to 1, which is very high as expected for this kind of BODIPY dye.

Biological evaluation

Radioligand binding studies

The synthesized model compounds **25-28** as well as the fluorescent ligands **29-33** were investigated in radioligand binding studies at the human A_{2B}AR stably expressed in Chinese hamster ovary (CHO) cells versus the antagonist radioligand [^{3}H]PSB-603 (Table 1). In order to assess the compounds' selectivity, radioligand binding studies at A_1AR, A_{2A}AR and A_3ARs were additionally performed using the following radioligands: [^{3}H]CCPA (A_1), [^{3}H]MSX-2 (A_{2A}), and [^{3}H]PSB-11 (A_3). For comparison, data for the unlabeled standard A_{2B}AR antagonist 8-(4-(4-(4-chlorophenyl)piperazine-1-sulfonyl)phenyl)-1-propylxanthine (**34**, PSB-603) and the nonselective antagonist caffeine (**35**), obtained in the same assay, are provided (see Table 1).

All tested model compounds displayed high affinity for the A_{2B}AR with K_i values in the low nanomolar range. The model compound with a linker length of four methylene units was the most potent A_{2B} antagonist (**28**, K_i = 3.30 nM), however derivatives with a methylene or an ethylene linker were similarly potent (**25**, K_i 7.00 nM; **26**, K_i 7.45 nM). Only the compound with a propylene chain appeared to be somewhat less potent **27**, K_i 27.9 nM, 8-fold difference compared to **28**. All model compounds were shown to be highly (> 150-fold) selective versus the A_{2A}AR subtype. Selectivity versus the A_{3A}AR was also high (> 100-fold) for most compounds with the exception of **25**, the derivative with the methylene linker, which still displayed 38-fold selectivity for A_{2B} over A_3. However, selectivity appeared to be much lower versus the A_1AR,

although in this case – like in the case of the A_{2A}AR – data for the human A_{2B}AR were compared with data obtained at the rat A_1AR. This appeared to be accurate enough for a preliminary assessment of model compounds, but may actually underestimate the compounds' A_{2B} selectivity for the human A_{2B}AR since xanthine derivatives are often more potent at rat as compared to human A_1ARs.[49] In summary, compound **26** showed the best profile among the tested model compounds, i.e. high potency, short linker chain, and high selectivity, at least versus A_{2A} and A_3ARs, and thus an ethylene linker appeared to be most promising. Therefore, we synthesized the corresponding BODIPY-labeled xanthine derivative **29**. In addition, we prepared the fluorescent ligands **30**-**33** with longer linker lengths up to ten methylene units and evaluated them in radioligand binding assays (see Table 1).

Table 1. Adenosine receptor binding affinities

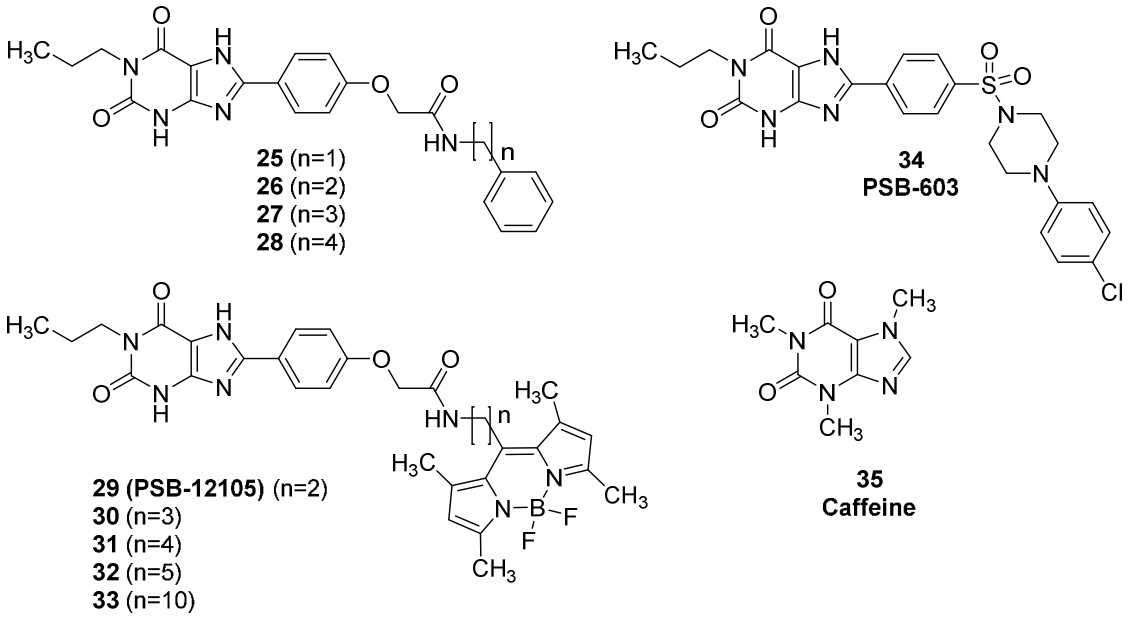

Compound	n	K_i ± SEM (nM)			
		A_1AR [^{3}H]CCPA	A_{2A}AR [^{3}H]MSX-2	A_{2B}AR [^{3}H]PSB-603	A_3AR [^{3}H]PSB-11

		Human recombinant (h) or rat brain cortex (r)	Human recombinant (h) or rat brain striatum (r)	Human (h), rat (r) or mouse (m) recombinant	Human recombinant (h)
34 (PSB-603)	-	> **10,000** (h, r)[55]	> **10,000** (h, r)[55]	**0.553** (h)[55] **0.351** (m)[55]	> **10,000** (h)[56]
35 (Caffeine)	-	> **10,000** (h, r)	**23,400** (h)[57a] **28,700** (r)	**33,800** (h)[55] **30,000** (r)[56] **23,000** (m)[56]	**> 13,300** (h)[49]
25	1	**27.2** ± 4.1 (r)	**> 10,000** (r)	**7.00** ± 1.39 (h)	**266** ± 61 (h)
26	2	**7.85** ± 2.46 (r)	**> 10,000** (r)	**7.45** ± 2.43 (h)	> **10,000** (h)
27	3	**35.3** ± 5.7 (r)	**> 10,000** (r)	**27.9** ± 9.1 (h)	**2,990** ± 438 (h)
28	4	**29.6** ± 4.0 (r)	**498** ± 132 (r)	**3.30** ± 1.24 (h)	**1,410** ± 234 (h)
29 (PSB-12105)	2	≥ **10,000** (h) **422** ± 35 (r)	> **10,000** (h) > **10,000** (r)	**1.83** ± 0.76 (h) **0.180** ± 0.067 (r) **1.32** ± 0.26 (m)	**> 10,000** (h)
30	3	**168** ± 13 (r)	**2150** ± 392 (r)	**11.6** ± 3.4 (h)	**904** ± 155 (h)
31	4	**178** ± 23 (r)	**1570** ± 277 (r)	**24.4** ± 6.6 (h)	**719** ± 116 (h)
32	5	**714** ± 272 (h) **77.9** ± 12.8 (r)	**58.7** ± 14.4 (h) **477** ± 68 (r)	**5.90** ± 2.16 (h)	**4550** ± 858 (h)
33	10	> **10,000** (h) **227** ± 21 (r)	**1600** ± 140 (h) > **10,000** (r)	**7.82** ± 1.94 (h)	≥ **10,000** (h)

[a]Human A_{2A}AR vs. [^{3}H]8-cyclopentyl-1,3-dipropylxanthine ([^{3}H]DPCPX)

As already observed for the phenyl-substituted model compounds **25**-**28**, the linker length had also only a minor effect on A_{2B} affinity of the BODIPY-labeled xanthines. All derivatives, including the ones with a longer C5- (**32**) or C10-linker (**33**), displayed high A_{2B}AR affinity with low nanomolar K_i values. However, the SARs showed subtle differences, not only regarding A_{2B}

affinity but also with respect to selectivity versus the other AR subtypes. The A_{2B}-selectivity of the BODIPY-labeled xanthines versus the A_1AR was generally higher (compare **26**/**29**, **27**/**30** and **28**/**32**) than that of the model compounds. The fluorescent ligand **29** showed the highest A_{2B} affinity of all investiged compounds with a K_i value of 1.83 nM for the human A_{2B}AR (see Table 1 and Figure 4A). Moreover, similarly to one of the most potent and selective A_{2B} antagonists, the standard antagonist **34** (for structure and data see Table 1), **29** was found to be highly (>1,000-fold) selective versus the human A_1, A_{2A} and A_3AR subtypes. In order to evaluate potential species differences, **29** was further examined in radioligand binding assays using membrane preparations of CHO cells stably overexpressing rat or mouse A_{2B}ARs, respectively. The fluorescent ligand **29** also displayed high affinity for rat and mouse A_{2B}ARs, with K_i values of 0.180 nM (rat A_{2B}AR) and 1.32 nM (mouse A_{2B}AR) (Table 1, Figure S5, Figure S6 in Supporting Information). This means that **29** is similarly potent at A_{2B}ARs of all three species. Figure S6 summarizes the obtained radioligand binding data for the fluorescent A_{2B}AR antagonist **29**. Given the well-known fact that xanthine derivatives lacking a substituent at N3 are inactive at rodent A_3ARs[49] it can be concluded that **29** represents a very potent and highly selective fluorescent A_{2B}AR ligand which should not only be useful for studies in human cells and tissues, but also in rodent cells, tissues and animal models.

cAMP accumulation studies

As a next step, functional properties of the model compounds **25-27** and of the fluorescent ligand **29** were studied employing cAMP accumulation assays. The model compounds as well as the BODIPY-labeled xanthine derivative **29** inhibited agonist- (NECA-, 10 μM) -induced cAMP accumulation in A_{2B}AR expressing CHO cells in a concentration-dependent manner and to the

same maximal extent as the standard A_{2B}AR antagonist **34**. The fluorescent compound **29** showed an IC_{50} value of 262 nM, while the standard antagonist **34** displayed an IC_{50} value of 18.3 nM (see Figure 4B). The IC_{50} values determined for the model compounds were as follows: 135 nM for **25**, 141 nM for **26** and 174 nM for **27**. The apparently lower potency of the tested antagonists **25-27**, **29** and **34** in functional assays as compared to radioligand binding studies can be explained by the high agonist concentration that was used in the assay to stimulate the A_{2B}ARs, which required relatively high concentrations of the competitive antagonists to block its effect. These data clearly show that the model compounds as well as the fluorescent ligand **29** functionally behave as A_{2B}AR antagonists. Moreover, the most potent antagonist in radioligand binding studies, **34**, was also the most potent antagonist in the functional assay (K_i 0.553 nM; IC_{50} 18.3 nM).

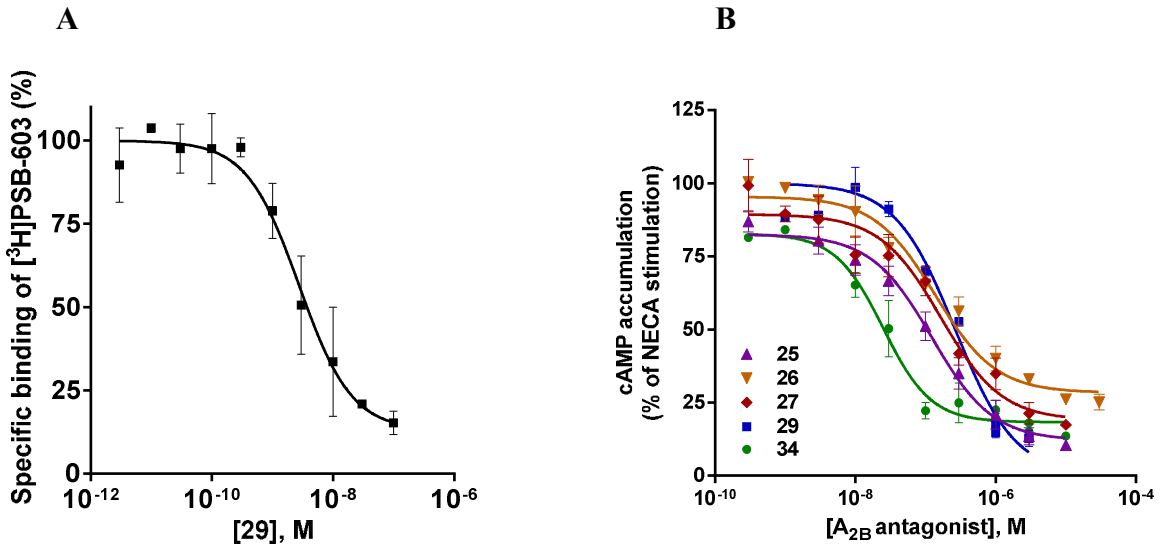

Figure 4. A. Competition binding experiments of **29** at membrane preparations of recombinant CHO cells expressing human A_{2B}ARs. A K_i value of **1.83** ± 0.76 nM was determined. Data points represent means ± SEM of three independent experiments. **B**. Concentration-dependent inhibition of NECA (10 µM)-induced cAMP accumulation by **25**, **26**, **27**, and **29** and by the

standard A_{2B}AR antagonist **34** in CHO cells expressing the human A_{2B}AR. IC_{50} values were 135 ± 45 nM (**25**), 141 ± 30 nM (**26**), 174 ± 38 nM (**27**), 262 ± 48 nM (**29**) and 18.3 ± 2.1 nM (**34**). Data points represent means ± SEM from three independent experiments performed in duplicates.

Confocal microscopy

Confocal microscopy was performed to investigate the imaging properties of the fluorescent ligand **29**. Incubation of CHO cells recombinantly expressing the human A_{2B}AR (CHO-A_{2B}) with **29** (100 nM) resulted in labeling of the cell membranes (Figure 5A), which was absent in the control experiments using wild-type (wt) CHO cells treated with **29** under the same conditions (Figure 5D). To further confirm that the observed labeling was A_{2B}AR-specific, the CHO-A_{2B} cells were pre-incubated with the selective A_{2B}AR antagonist **34**. In fact, pre-incubation with **34** (100 nM) for 30 min completely prevented membrane labeling (Figure 5B). Similarly, pre-treatment with 1,3-dipropyl-8-cyclopentylxanthine (DPCPX, 1 μM) led to reduced fluorescence although to a lower extent (Figure 5D).

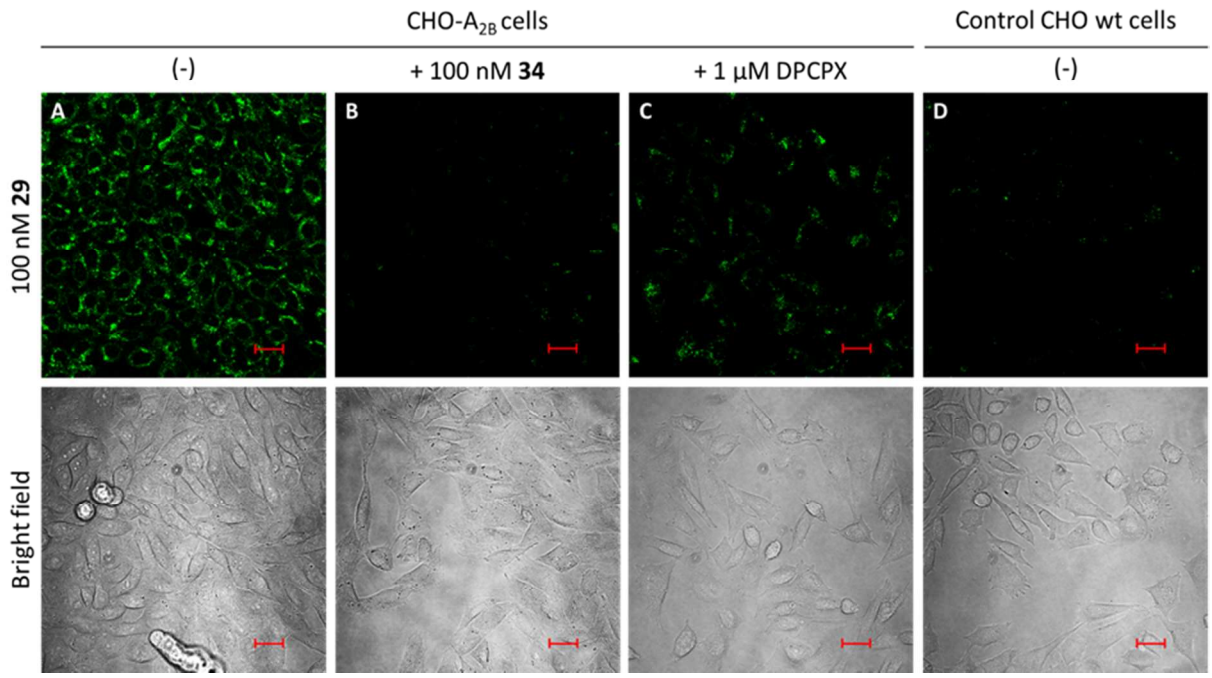

Figure 5. Confocal imaging. CHO-A_{2B} cells (**A-C**) were grown on sterile chambered coverslips and subsequently incubated with **29** (100 nM) for 15 min at 37°C, (**A**) in the absence, or (**B**) in the presence of **34** (100 nM, pre-incubation for 30 min), or (**c**) in the presence of DPCPX (1 µM, preincubation for 30 min). As a control, CHO wt cells were treated with **29** under the same conditions (**D**). All confocal images and their corresponding transmitted light images (lower row) were taken using identical microscope settings regarding laser power, detector offset and gain. Images shown are from a single representative experiment out of three similar experiments. Scale bars = 100 µm.

Flow cytometry-based A_{2B}AR binding assays

Finally, we utilized the new fluorescent A_{2B}AR antagonist **29** to develop a homogenous flow cytometry-based fluorescence binding assay for the A_{2B}AR using living CHO cells recombinantly expressing the human A_{2B}AR. The optimal cell number in a sample vial providing the best signal window was determined to be in a range of 250,000 to 500,000 cells per vial.

Using Hank's balanced salt solution (HBSS) as a buffer was found to result in a higher fluorescence signal to noise ratio than Dulbecco's Modified Eagle Medium (DMEM-F12) and was therefore utilized as an incubation buffer in all subsequent experiments. For the measurement of nonspecific binding various AR ligands were tested, namely the A_1-selective AR antagonist DPCPX, the non-selective AR agonist NECA and the A_{2B}-selective AR antagonist PSB-603 (**34**). In these preliminary experiments, the unlabeled ligands were co-applied with the fluorescent ligand **29**. DPCPX was not regarded suitable for the determination of nonspecific binding, since in initial experiments we could not detect specific binding of **29** using DPCPX as a competitor. Contrary to our expectations, the fluorescence signal even increased in the presence of DPCPX. The reason for that might be the formation of aggregates between the fluorescent ligand **29** and DPCPX at higher DPCPX concentration (10 μM) disturbing the assay.[58] However, as expected, the nonselective A_{2B}AR agonist NECA as well as the highly selective A_{2B}AR antagonist **34** were clearly able to displace the fluorescent ligand **29** from its binding site and were thus found to be suitable for the determination of the nonspecific binding. In notransfected CHO-K1 cells no specific binding could be determined showing that the detected specific binding was merely due to the A_{2B}AR, and **29** specifically labels A_{2B}ARs. Subsequently, we performed competition binding experiments and determined concentration-dependent inhibition of binding of the fluorescent A_{2B}AR ligand **29 (**1 nM) by the standard antagonist **34** (Figure 6D). An IC_{50} value of 0.534 nM was calculated for **34**, which is in excellent agreement with its K_i value determined in radioligand binding assays (0.553 nM).[55]

After initial FACS experiments performed on a BD LSRII flow cytometer, we subsequently adapted it to a 96-well format using a guava easyCyte HT sampling flow cytometer (for details

see Experimental Section). In preliminary measurements we observed fast association kinetics for **29**. Therefore, we subsequently changed the protocol and pre-incubated the cells with the compounds that were investigated for competition. This change in experimental conditions allowed us to observe displacement of **29** by DPCPX, which had not inhibited **29** binding in preliminary FACS experiments in which both compounds had been co-administered. The standard A_{2B} antagonist **34** displayed an IC_{50} value of 0.739 nM which is not significantly different from the IC_{50} value of 0.534 nM previously determined in flow cytometry assays without pre-incubation. Thus, pre-incubation does not appear to be required for all antagonists, it likely depends on the binding kinetics of each compound in comparison to the fluorescent ligand. In all subsequent experiments, the antagonists were pre-incubated for 30 min at 37°C with the cells before adding the fluorescent ligand, followed by an additional incubation for 20 min. Various standard A_{2B}AR antagonists were examined for their ability to inhibit the binding of **29**. As shown in Figure 6B, all tested A_{2B}AR antagonists displaced **29** with IC_{50} values ranging between 1 and 100 nM.

These results indicate that the new flow cytometry-based competition binding assay with the newly developed A_{2B}-selective fluorescent antagonist **29** provides a convenient alternative method to radioligand binding assays, potentially adaptable to high-throughput screening. Thus, our fluorescent A_{2B}AR antagonist **29** represents a new powerful tool for A_{2B}AR studies.

A **B**

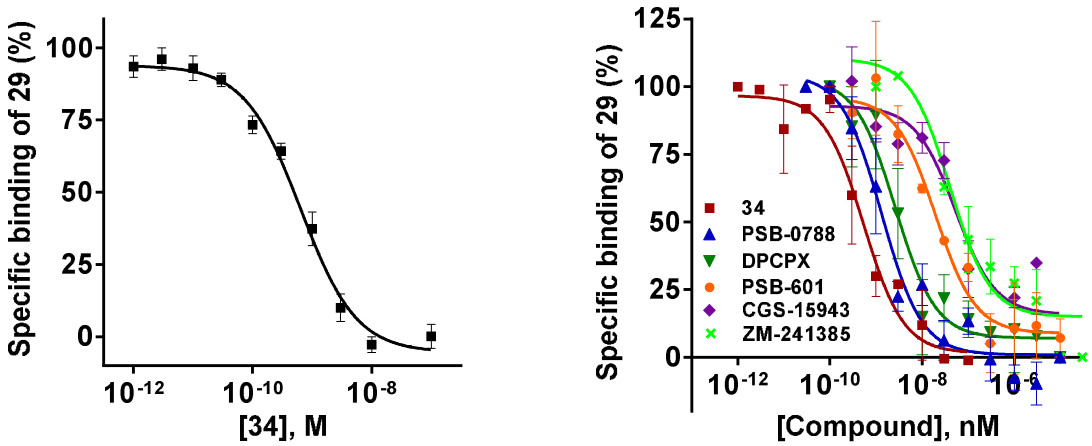

Figure 6. Fluorescence competition binding experiments using CHO cells recombinantly expressing human A_{2B}ARs. **A**. Experiments were performed using a BD LSRII flow cytometer. The fluorescent ligand **29** was displaced by the A_{2B}-selective standard antagonist **34** in a concentration-dependent manner as determined by flow cytometry. An IC_{50} value of 0.534 ± 0.155 nM was determined for **34**. Data points represent means ± SEM from 5 independent experiments, each performed in duplicates. **B**. Experiments were performed in a 96-well format using a guava easyCyte HT sampling flow cytometer. The determined IC_{50} values were as follows: 0.739 ± 0.622 nM (**34**), 1.06 ± 0.71 nM ((8-(4-(4-(4-chlorobenzyl)piperazine-1-sulfonyl)phenyl)-1-propylxanthine (PSB-0788)), 3.80 ± 1.15 nM (8-cyclopentyl-1,3-dipropylxanthine (DPCPX)), 23.5 ± 12.7 nM (8-[4-(4-benzylpiperazide-1-sulfonyl)phenyl]-1-propylxanthine (PSB-601)), 60.7 ± 27.4 nM (9-chloro-2-(2-furanyl)[1,2,4]triazolo[1,5-*c*]quinazolin-5-amine (CGS-15943)), and 94.9 ± 76.6 nM (4-(2-[7-amino-2-(2-furyl)-[1,2,4]triazolo-[2,3-*a*][1,3,5]triazin-5-ylamino]ethyl)-phenol (ZM-241385)). Data points represent means ± SEM from 3-5 independent experiments, each performed in duplicates.

All values determined by the fluorescence-based competition assay using flow cytometry were in the same range as those previously determined by radioligand binding studies.[55,56]

Molecular modeling studies

The design of the potent and selective fluorescent A_{2B}AR antagonist **29** was supported by docking studies using a homology model of the human A_{2B}AR. We had previously constructed such a model[50] based on the crystal structure of the human A_{2A}AR (2.6 Å) in complex with the subtype-selective antagonist ZM241385 (PDB ID: 3EML).[59] In the present study, the homology model of the human A_{2B}AR was updated using the crystal structure of the human A_{2A}AR obtained at a higher resolution (1.8 Å) in complex with ZM241385 (PDB ID: 4EIY) as a template.[60] The binding pose of **29** predicted by the docking studies showed that the xanthine core with the attached 8-phenyl group closely overlaps with the crystallographic pose of xanthine amine congener (XAC, **36**) observed in the X-ray structure its complex with the A_{2A}AR with (PDB ID: 3REY, resolution 3.31 Å) (see Figure 7).[61] A recently reported crystallographic pose for another xanthine derivative, which was originally developed by our group, 1-butyl-8-(hexahydro-2,5-methanopentalen-3a(1*H*)-yl)-3,7-dihydro-3-(3-hydroxypropyl)-1*H*-purine-2,6-dione (PSB-36, **37**, Figure 7), in complex with the human A_{2A}AR showed a different, alternative binding mode: the hydroxypropyl substituent attached to the N3 of **37** pointed towards the position of the 8-phenyl substituent of the BODIPY-labeled **29**. The 8-(3-noradamantyl) residue of **37** was positioned between the C6-carbonyl and the N7-H of the xanthine core of XAC (**36**).[62] The reason for the shifted pose of the xanthine core can be explained by the larger substituents at N1 (butyl) and N3 (hydroxpropyl) in the 8-noradamantylxanthine derivative **37** as compared to **29** and **36**, which would cause a steric clash with Met270.

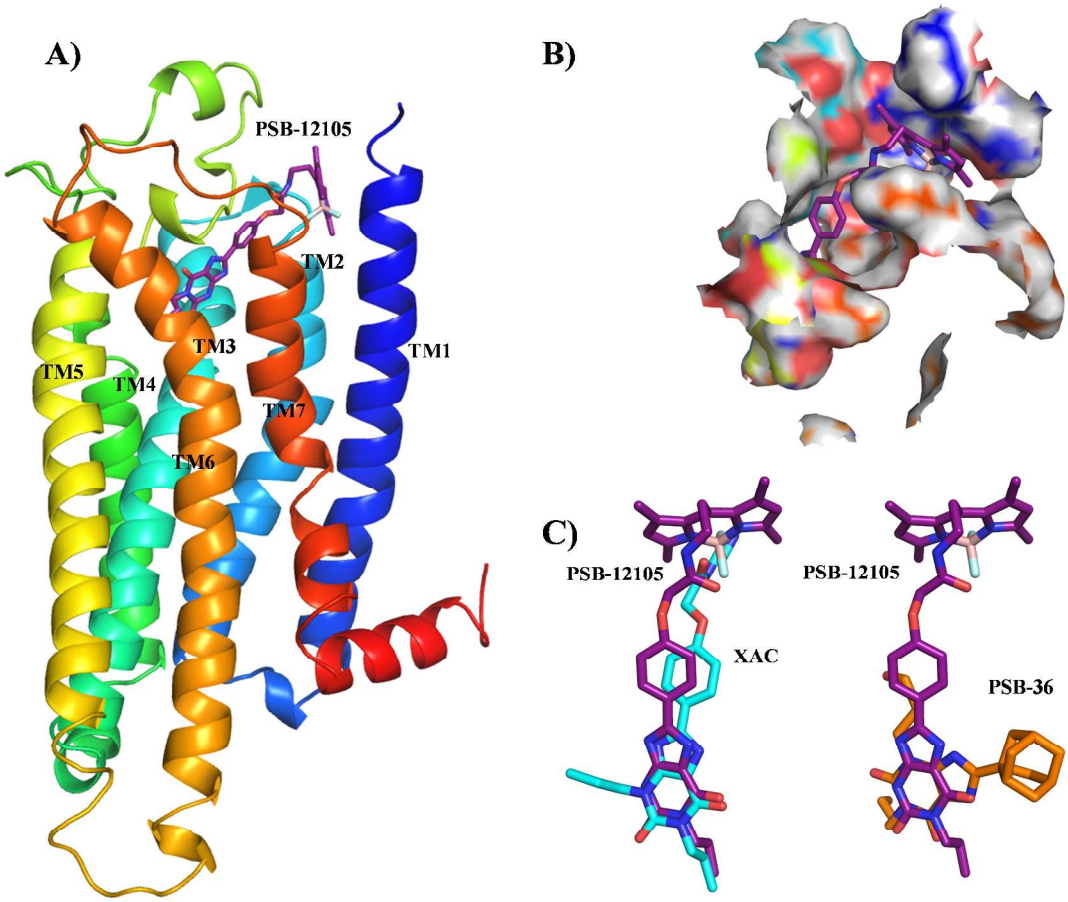
A)
PSB-12105
TM2
TM3
TM1
TM5
TM4
TM7
TM6
B)
C)
PSB-12105
XAC
PSB-12105
PSB-36

D)

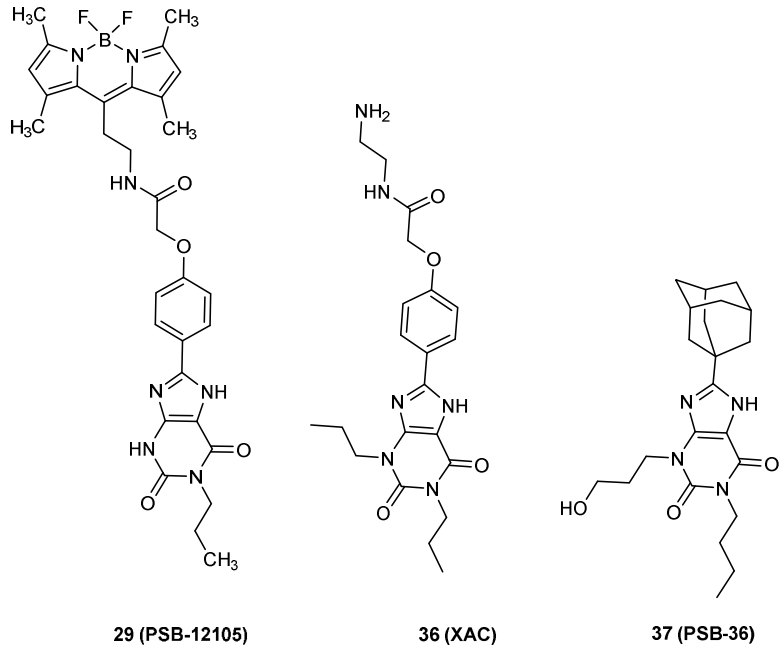

Figure 7. Proposed binding mode of 29. (**A**) Docking pose of the antagonist **29** (represented in stick and carbon atoms colored in magenta) in the active site of the A_{2B}AR (in ribbon presentation and colored in continuum spectrum). (**B**) Docked pose of **29** in the binding pocket of the A_{2B}AR. (**C**) The predicted pose of **29** observed in the performed docking studies compared to the binding pose of XAC (**36**) (carbon atoms colored in cyan, PDB ID: 3REY) and PSB-36 (**37**) (carbon atoms colored in orange, PDBID:5N2R) as observed in the X-ray structures in complex with the A_{2A}AR. (**D**) Comparison of the structures of **29** (PSB-12105), **36** (XAC) and **37** (PSB-36). Oxygen atoms are colored in red, nitrogen atoms in blue, hydrogen atoms in silver white, boron atoms in light pink and fluorine atoms in light cyan.

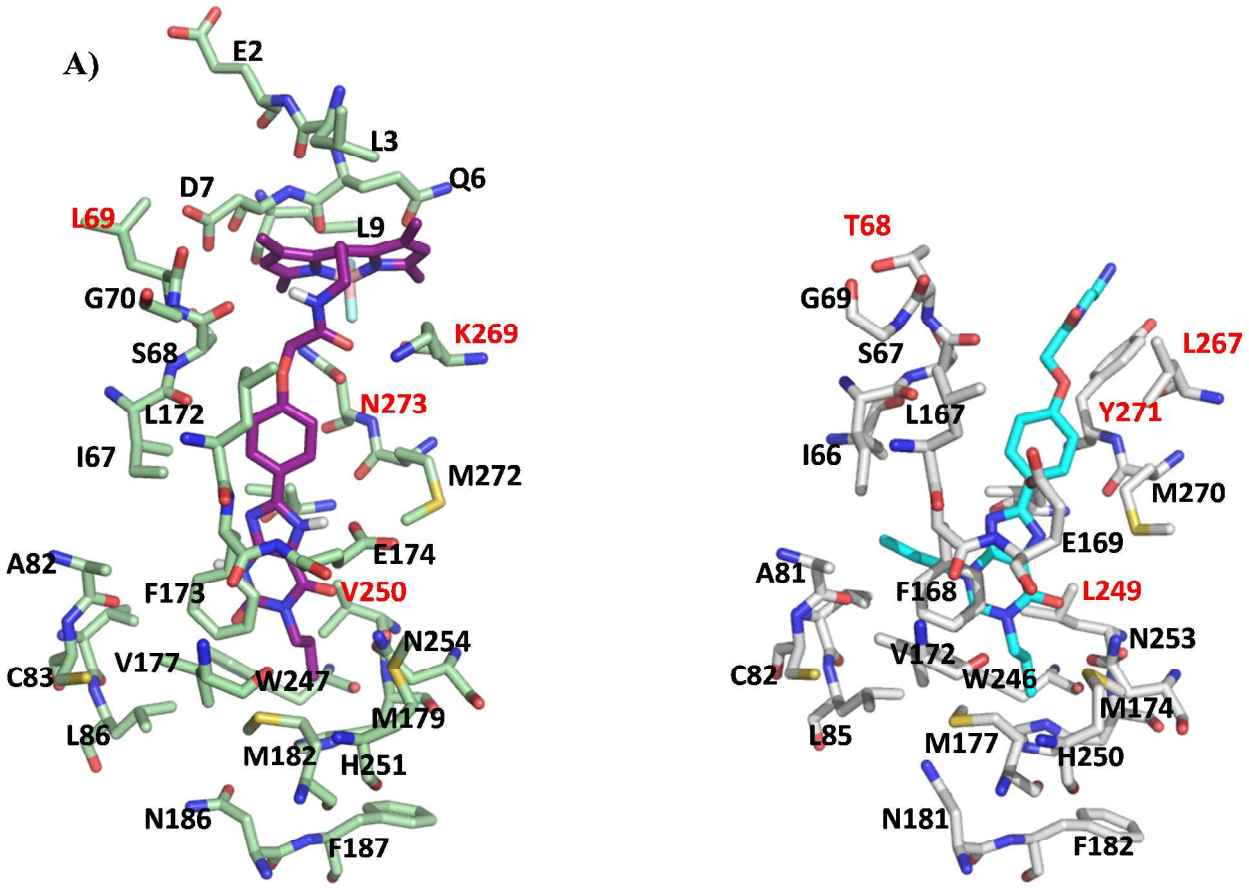
A)
E2
L3
Q6
D7
L69
L9
G70
K269
S68
N273
L172
I67
M272
E174
A82
F173
V250
N254
V177
C83
W247
M179
L86
M182
H251
N186
F187
T68
G69
L267
S67
L167
Y271
I66
M270
E169
A81
F168
L249
N253
V172
C82
W246
M174
L85
M177
H250
N181
F182

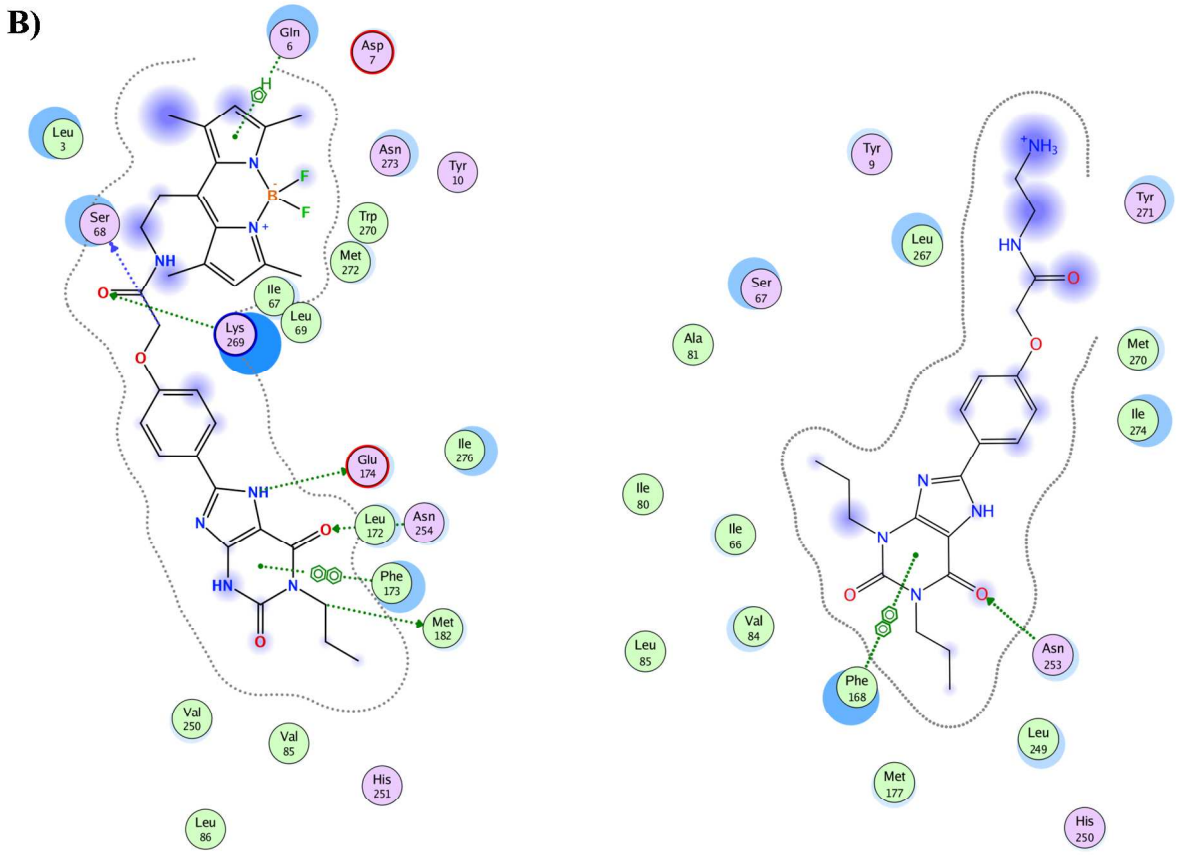

Figure 8. Proposed binding interactions of 29. (**A**) The docked pose of **29** (in magenta) and the amino acid residues in the binding pocket of the A_{2B}AR (pale green) are compared to **36** (XAC) (cyan) and the amino acid residues in the binding pocket of the A_{2A}AR. Amino acids differing in A_{2A}AR and A_{2B}AR are colored in red. (**B**) A 2D interaction diagram of compound **29** with the human A_{2B}AR and of **36** with the human A_{2A}AR are depicted. The binding pose representation and the color code is as described in Figure 7.

As shown in Figure 8, the heterocyclic core structure of **29** likely forms one of the key π-π stacking interactions with Phe173 and utilizes the hydrophobic surface provided by Ile276 in the A_{2B}AR. The C6-carbonyl and the N7-H of the xanthine core form key hydrogen bond interactions with Asn254 and Glu174, respectively. The residues Phe173, Asn254 and Ile276 are conserved among the different subtypes of human ARs, and Glu174 is common in three subtypes (A_1, A_{2A}, A_{2B}), but replaced by valine in the A_3AR at the corresponding position (Val169, A_3AR numbering, see Sequence Alignment in Supplementary Figure S9). In the crystal structure of the human A_{2A}AR complexed with XAC, the corresponding amino acid for Glu174 in the A_{2B}AR (Glu169 in A_{2A}AR numbering) is rotated around by 150° and does not form hydrogen bond interactions with the N7-H of the xanthine core of XAC. Instead, in the crystal structure with ZM541385, Glu169 of the A_{2A}AR forms an interaction with the free exocylic amino group (NH_2) of the heterocyclic core. These observations further support the selection of the high resolution crystal structure of the A_{2A}AR (4EIY.pdb) as a template for the homology model of the A_{2B}AR. The propyl substituent at N1 of the xanthine derivative **29** binds within the pocket formed by Met182, Val250 and His251. Among these residues, Val250 is unique for the A_{2B}AR which might contribute to the selectivity of the compounds for the A_{2B}AR. The phenyl group at C8 is co-planar with the heterocyclic core and forms a weak hydrophobic interaction with Ile67. The linker chain length contributes to the fold, and the carboxamide group in the linker forms hydrogen bonding interactions with the main chain of Ser68 and the side-chain of Lys279. The interaction between the keto group of the carboxamide function and Lys279 possibly contributes tothe selectivity of compound **29** for the A_{2B}AR, in addition to Val250 in the heterocyclic core binding pocket. In comparison to other subtypes of human ARs, both Val250 and Lys279 are unique for the A_{2B}AR (Figure 8). Additionally, another unique residue, namely Asn273 in the

A_{2B}AR, is in closer proximity to Lys279 and near the binding pocket of **36**. According to the model, the BODIPY residue of **29** binds within the pocket formed by the residues Leu3, Gln6, Asp7, and Leu69 and extends to the surface between transmembrane regions TM1 and TM7 of the receptor. Among these residues interacting with BODIPY, Gln6 and Asp7 are unique for the A_{2B}AR and might contribute to the compound's selectivity. Thus, the docking studies provide a rational explanation for the interaction of **29** with the A_{2B}AR and for its selectivity versus the other AR subtypes, which will have to be confirmed by future mutagenesis studies.

CONCLUSIONS

In summary, we have developed a fluorescent antagonist for the A_{2B}AR, compound **29**, in which a BODIPY fluorophore is integrated into the A_{2B} antagonist pharmacophore structure. The fluorescent ligand shows equally high A_{2B}AR affinity of around 1-2 nM for human, rat and mouse A_{2B}ARs combined with high A_{2B}AR subtype selectivity. It possesses excellent fluorescence characteristics, in particular high fluorescence quantum yields. A refined homology model of the human A_{2B}AR was built based on a recently published high-resolution X-ray structure of the A_{2A}AR, and the binding of **29** to the orthosteric binding site was rationalized. The fluorescent antagonist ligand **29** was successfully used to establish a straightforward homogeneous fluorescence binding assay using flow cytometry. The new A_{2B}AR fluorescence assay was found to be reliable and may be used to substitute radioligand binding studies. Future studies will be directed towards evaluating **29** for further applications, e.g. in native cells and tissues.

EXPERIMENTAL SECTION

General methods. All reactions were performed in dry solvents, unless otherwise indicated. Dichloromethane (DCM) was freshly distilled over CaH_2 prior to use. All other reagents were used as obtained from various providers (Acros, Aldrich, Fluka, Merck, Sigma) unless otherwise noted. The reactions were monitored by thin layer chromatography (TLC) using silica gel-coated aluminum sheets (0.2 mm layer, nano-silica gel 60 with fluorescence indicator UV_{254} (Merck, Darmstadt, Germany)). Column chromatography was performed on Merck silica gel 60 (mesh size 0.040-0.063 mm). Melting points were measured in open capillary tubes on a Wepa Apotec capillary melting point apparatus (Wepa, Höhr-Grenzhausen, Germany) and are uncorrected. NMR spectra were recorded on a Bruker Avance DRX 500 spectrometer. ^{1}H- and ^{13}C NMR data were collected on a Bruker Avance 500 MHz NMR spectrometer at 500 MHz (^{1}H), or 125 MHz (^{13}C), respectively. The employed solvents are given below. Data are presented as follows; chemical shift, multiplicity (s, singlet; d, doublet; dd, double doublet; t, triplet; q, quartet; m, multiplet; br, broad; br s, broad singlet), coupling constant, and integration.

The purities of isolated products were determined by ESI-mass spectra obtained on an LCMS instrument (Applied Biosystems API 2000 LCMS/MS, HPLC Agilent 1100) using the following procedure: the compounds were dissolved at a concentration of 1.0 mg/mL in acetonitrile containing 2 mM ammonium acetate. Then, 10 μL of the sample were injected into an HPLC column (Macherey-Nagel Nucleodur® 3 μ C18, 50 x 2.00 mm). Elution was performed with a gradient of water/acetonitrile (containing 2 mM ammonium acetate) from 90:10 to 0:100 for 20 min at a flow rate of 300 μL/min, starting the gradient after 10 min. UV absorption was detected from 200 to 950 nm using a diode array detector (DAD). Purity of all compounds was determined at 254 nm. The purity of the compounds was ≥95%.

Determination of fluorescent quantum yields

Fluorescent quantum yield measurements were determined by a Cary Eclipse fluorescence spectrophotometer, Varian, and a UV/Vis spectrometer lambda 25, Perkin Elmer Instruments. The slit width was 5 nm for excitation and emission. Relative quantum yields were obtained by comparing the areas under the corrected emission spectrum. The following equation was used to calculate the quantum yield.

$$\Phi_x = \Phi_{st} \cdot \frac{I_x}{I_{st}} \cdot \frac{A_{st}}{A_x} \cdot \frac{\eta_x^2}{\eta_{st}^2}$$

Where Φ_{st} is the reported quantum yield of the standard, I is the integrated emission spectrum, A the absorbance at the excitation wavelength and η the refractive index of the used solvents. The subscript x denotes unknown and st denotes standard. Rhodamine 6G (Φ = 0.94 in ethanol) was used as a standard.

6-Amino-3-propyluracil (19)

6-Aminouracil (6.40 g, 50 mmol) was refluxed for 2h with an excess of HMDS (10.51 g, 65 mmol) and a catalytic amount of $(NH_4)_2SO_4$ until a clear solution is obtained. The excess of HMDS was distilled off. The mixture was cooled to 0°C and propyl bromide (12.30 g, 0.1 mol) and a catalytic amount of I_2 was added. After the initial exothermic reaction was completed the reaction mixture was refluxed for 16h. To the reaction mixture a saturated aqueous $NaHCO_3$ solution was given in small portions under ice cooling. The formed precipitate was filtered off and washed with hot water. The crude product was purified by column chromatography with DCM:MeOH = 9:1 (v/v). Yellow solid (6.85 g, 81 % yield). Analytical data were consistent with the previously reported data.[53]

6-Amino-5-nitroso-3-propyluracil (20)

A solution of **19** (8.46 g, 50 mmol) was dissolved in 250 mL of a 50 % aq. acetic acid solution. The reaction mixture was heated up to 70°C. Then 6.9 g of $NaNO_2$ (100 mmol) was added in small portions over a period of 30 min. The mixture was stirred for 30 min and was then allowed to cool down to room temperature. The precipitate was filtered off and washed with water. Orange solid (7.03 g, 71 % yield). Analytical data were consistent with the previously reported data.[54]

5,6-Diamino-3-propyluracil (21)

Compound **20** (1.98 g, 10 mmol) was dissolved in MeOH and a catalytic amount of PtO_2 was added. The solution was stirred at rt for 2h under an atmosphere of H_2 (42 psi). The reaction mixture was subsequently filtered and the product was concentrated and used without any further purification due to its instability. Brown oil (1.81 g, 98 % yield). Analytical data were consistent with the previously reported data.[54]

6-Amino-5-(4-methoxycarbonylmethoxybenzylidenamino)-3-propyluracil (22)

To a solution of **21** (516 mg, 2.8 mmol) dissolved in ethanol an equimolar amount of methyl-(4-formylphenoxy)acetate was added followed by a few drops of acetic acid. The reaction mixture was stirred at room temperature for 1h and then precipitated by the addition of ice-cold water. The product was filtered off. White solid (928 mg, 92 % yield). Analytical data were consistent with the previously reported data.[52]

8-(4-Methoxycarbonylmethoxy)phenyl-1-propylxanthine (23)

Compound **22** (1.58 g, 4.4 mmol) was dissolved in 120 mL of thionyl chloride and stirred for 2h at 70°C. Then excess thionyl chloride was distilled off and the residue was suspended in ice-water. The residue was filtered off and washed with water. The crude product was

recrystallized by dissolving it in DMF followed by dropwise addition of water. White solid (1.42 g, 90 % yield). Analytical data were consistent with the previously reported data.[52]

8-(4-Carboxymethyloxyphenyl)-1-propylxanthine (24):

Compound **23** (0.366 g, 1 mmol) was dissolved in 5 mL DMF, and 5 mL of 0.1 *N* aq. Na_2CO_3 solution was added. The reaction mixture was stirred at 100°C for 30 min. The mixture was then concentrated and filtered. The filtrate was acidified (pH = 3) by addition of concentrated aq. HCl solution. The formed precipitate was filtered off. White solid (286 mg, 83 % yield). Analytical data were consistent with the previously reported data.[52]

General procedure for the amide coupling yielding 25-28

Compound **24** (96 mg, 0.28 mmol) was dissolved in 5 mL of DMF, and *N*-methylmorpholine (34 µL, 0.31 mmol) was added. The mixture was stirred at rt for 5 min. Then the reaction mixture was cooled to -22°C and isobutyl chloroformate (37 µL, 0.28 mmol) was added. After 15 min the appropriate amine (0.28 mmol) was added and the mixture was stirred at rt for 3h. The solvent was removed under reduced pressure and the crude product was purified by column chromatography using DCM:MeOH (40:1) as eluent.

1-Propylpurine-2,6-dione-8-(phenoxyacetic acid 4-phenylbenzylamide) (25)

White solid (31 mg; 25 % yield), mp > 300°C. ^{1}H-NMR (500 MHz, DMSO-d_6): δ = 0.86 (t, J = 8.1 Hz, 3H), 1.59 (m, 2H), 3.81 (m, 2H,), 4.35 (d, J = 7,3 Hz, 2H), 4.63 (s, 2H), 7.03 (d, J = 7.9 Hz, 2H), 7.17-7.28 (m, 5H), 8.02 (d, J = 7,8 Hz, 2H), 8.62 (t, J = 7.9 Hz, 1 H), 11.80 (s, 1H), 13.44 (s, 1H); ^{13}C-NMR (125 MHz, DMSO-d_6): δ = 67.2, 107.4, 115.3, 122.2, 125.8, 127.3, 128.1, 128.3, 139.4, 147.9, 151.1, 154.9, 159.4, 167.6. MS (ESI) (*m/z)*: 434.1 $[M+H]^+$.

1-Propylpurine-2,6-dione-8-(phenoxyacetic acid 4-phenylethylamide) (26)

White solid (69 mg; 55 % yield), mp > 300°C. ^{1}H-NMR (500 MHz, DMSO-d_6): δ = 0.86 (t, J = 8.1 Hz, 3H), 1.57 (sex, J = 7.3 Hz, 2H), 2.76 (t, J = 7.9 Hz, 2H,), 3.35 (dt, J = 7,3 Hz, J = 4.9 Hz, 2H), 3.81 (t, J = 7.9 Hz, 2H), 4.53 (s, 2 H), 7.03 (d, J = 7.9 Hz, 2H), 7.17-7.28 (m, 5H), 8.02 (d, J = 7.9 Hz, 2H), 8.14 (t, J = 7.9 Hz, 1 H), 11.80 (s, 1H), 13.44 (s, 1H); ^{13}C-NMR (125 MHz, DMSO-d_6): δ = 22.5, 29.9, 32.6, 38.2, 39.2, 67.5, 115.3, 125.8, 128.3, 129.0, 131.3, 131.2, 141.8, 142.2, 151.1, 159.4, 167.1. MS (ESI) (*m/z)*: 448.3 $[M+H]^+$.

1-Propylpurine-2,6-dione-8-(phenoxyacetic acid 4-phenylpropylamide) (27)

White solid (113 mg; 88 % yield), mp > 300°C. ^{1}H-NMR (500 MHz, DMSO-d_6): δ = 1.75 (m, 2H), 2.53 (t, J = 7.9 Hz, 2H), 3.15 (dt, J = 7.9 Hz, J = 6.4 Hz, 2H), 3.81 (t, J = 7.9 Hz, 2H), 4.55 (s, 2 H), 7.06 (d, J = 7.9 Hz, 2H), 7.14-7.25 (m, 5H), 8.02 (d, J = 7.9 Hz, 2H), 8.09 (t, J = 7.9 Hz, 1 H), 11.80 (s, 1H), 13.43 (s, 1H); ^{13}C-NMR (125 MHz, DMSO-d_6): δ = 22.5, 28.5, 29.9, 31.0, 38.2, 67.6, 107.4, 115.3, 122.2, 125.8, 128.0, 128.3, 128.6, 129.0, 142.2, 147.9, 151.1, 154.9, 159.4, 167.1. MS (ESI) (*m/z)*: 462.1 $[M+H]^+$.

1-Propylpurine-2,6-dione-8-(phenoxyacetic acid-4-phenylbutylamide) (28)

White solid (90 mg; 68 % yield), mp > 300°C. ^{1}H-NMR (500 MHz, DMSO-d_6): δ = 2.54 (t, J = 7.9 Hz, 2H), 3.17 (dt, J = 7.9 Hz, J = 6.7 Hz, 2H), 3.81 (t, J = 7.9 Hz, 2H), 4.53 (s, 2 H), 7.06 (d, J = 7.9 Hz, 2H), 7.12-7.24 (m, 5H), 8.01 (d, J = 7.9 Hz, 1 H), 8.07 (t, J = 7.9 Hz, 2H), 11.80 (s, 1H), 13.44 (s, 1H); ^{13}C-NMR (125 MHz, DMSO-d_6): δ = 18.7, 28.5, 29.9, 34.9, 38.2, 41.5, 67.6, 107.4, 115.3, 122.2, 125.7, 128.3, 128.4, 131.9, 142.2, 147.9, 150.2, 151.1, 154.9, 159.4, 167.1. MS (ESI) (*m/z)*: 475 $[M+H]^+$.

General procedure for the amide coupling yielding 29 and 32

Compound **24** (0.28 mmol) was dissolved in 5 mL of DMF, and HCTU (0.28 mmol) and HOBt (0.28 mmol) were added. After the addition of *N*-methylmorpholine (0.31 mmol) the reaction mixture was stirred for 1 min. Then the appropriate amino-substituted BODIPY derivative (**13** or **16**, 0.28 mmol), dissolved in 5 mL of DMF, was added. The solution was stirred for 16 h. Then the solvent was removed under reduced pressure. The residue was purified by column chromatography using DCM/MeOH (40:1) as eluent.

General procedure for the amide coupling yielding 30, 31 and 33

Compound **24** (0.2 mmol) was dissolved in 5 mL of DMF. After the addition of *N*-methylmorpholine (0.20 mmol) the reaction mixture was stirred for 5 min at rt. Then the reaction was cooled to -22 °C and isobutyl chloroformate (0.20 mmol) was added. After 15 min the appropriate amino-substituted BODIPY derivative (**14**, **15** or **17**, 0.20 mmol) was added. The solution was stirred for 3h at rt. Then the solvent was removed under reduced pressure. The residue was purified by column chromatography using DCM/MeOH (40:1) as eluent.

4-(1-Propyl-2,6-dioxo-2,3,6,7-tetrahydro-1*H*-purine-8-yl)-*N*-[2-(4,4-difluoro-1,3,5,7-tetramethyl-4-bora-3*a*,4*a*-diaza-*s*-indacen-8-yl)-etyl]phenoxyacetamide (29)

Orange solid (65 mg, 40 % yield), mp > 300°C. ^{1}H-NMR (500 MHz, DMSO-d_6): δ = 0.87 (m, 3H), 1.27 (m, 6H), 1.59-1.71 (m, 2H), 2.39 (s, 6H), 2.91 (m, 1H), 3.14 (m, 1H), 3.25 (m, 2H), 3.70-3.3.82 (m, 2H), 4.10-4.19 (m, 1H), 4.87 (s, 1H), 6.23 (s, 2H), 7.05 (d, J = 8.5 Hz, 1H), 7.26 (s, 1H), 7.65 – 7.71 (m, 1H), 8.01 (d, J = 7.9 Hz, 1H), 11.8 (br, 1H), 13.4 (br, 1H). ^{13}C-NMR (125 MHz, DMSO-d_6): δ = 13.9, 14.2, 16.0, 19.8, 29.9, 38.6, 67.2, 107.4, 115.3, 121.8, 128.1,

130.8, 140.9, 146.3, 147.9, 150.2, 151.1, 153.3, 154.8, 159.3, 167.6. MS (ESI) (*m/z):* 616.7 $[M-H]^+$.

4-(1-Propyl-2,6-dioxo-2,3,6,7-tetrahydro-1*H*-purine-8-yl)-*N*-[3-(4,4-difluoro-1,3,5,7-tetramethyl-4-bora-3*a*,4*a*-diaza-*s*-indacen-8-yl)-propyl]phenoxyacetamide (30)

Orange solid (29 mg, 22 % yield), mp 270°C. ^{1}H-NMR (500 MHz, DMSO-$d_{6,}$): δ = 1.54-1.59 (m, 4H, 2), 2.40 (s,12H, 10-CH_3 und 9-$CH_{3,}$ 12-CH_3 und 11-CH_3), 2.94 (m, 2H), 3.32 (dt, 2H), 3.80 (t, 2H), 4.56 (s, 2H), 7.07 and 8.05 (2d, 4H), 8.32 (t, 1H), 11.80 (s, 1H), 13.44 (s, 1H). ^{13}C-NMR (125 MHz, DMSO-d_6): δ = 11.3 (s, 1C), 13.9 (t, 2C), 15.95 (s, 2C), 22.5 (s, 1C), 28.5 (s, 1C), 29.9 (s, 1C), 38.2 (s, 1C), 41.5 (s, 1C), 67.5 (s, 1C), 107.37 (s, 1C, 5-C), 121.85 (s, 2C), 130.8 und 129.25 (2s, 2C), 140.9 (s, 2C), 146.8 (s, 1C), 147.9 (s, 1C), 150.2 (s, 1C), 151.1 (s, 1C, 2-C), 153.3 (s, 2C), 154.83 (s, 1C, 6-C), 167.65 (s, 1C), 115.3, 122.2, 128.0, 128.7, 159.3 (5s, 6C). MS (ESI) (*m/z*): 630.3 $[M-H]^-$.

4-(1-Propyl-2,6-dioxo-2,3,6,7-tetrahydro-1*H*-purine-8-yl)-*N*-[4-(4,4-difluoro-1,3,5,7-tetramethyl-4-bora-3*a*,4*a*-diaza-*s*-indacen-8-yl)-butyl]phenoxyacetamide (31)

Orange solid (20 mg, 17 % yield), mp 260°C. ^{1}H-NMR (500 MHz, DMSO-d_6): δ = 0.88 (t, 3H), 1.56-1.62 (m, 6H), 2.37 (s, 12H), 2.91 (m, 2H), 3.19 (m, 2H), 3.81 (m, 2H), 4.53 (s, 2H), 6.18 (s, 2H), 7.04 und 8.01 (2d, 4H), 8.11 (t, 1H), 11.81 (s,1H), 13.44 (s, 1H). ^{13}C-NMR (125 MHz, DMSO-d_6): δ = 11.3 (s, 1C), 14.1 (t, 2C), 15.9 (s, 2C), 27.0(s, 1C), 27.8 (s, 1C), 29.9 (s, 1C), 31.2 (s, 1C), 38.2 (s, 1C), 41.4 (s, 1C), 67.5 (s, 1C), 107.36 (s, 1C), 121.7 (s, 2C), 130.8 (s, 2C), 140.8 (s, 2C), 146.8 (s, 1C), 147.9 (s, 1C), 150.2 (s, 1C), 151.1 (s, 1C), 153.1 (s, 2C), 154.82 (s, 1C), 167.32 (s, 1C), 115.2, 122.2, 128.0, 128.7, 159.3 (5s, 6C). MS (ESI) (*m/z):* 644.7 $[M-H]^-$.

4-(1-Propyl-2,6-dioxo-2,3,6,7-tetrahydro-1*H*-purine-8-yl)-*N*-[5-(4,4-difluoro-1,3,5,7-tetramethyl-4-bora-3*a*,4*a*-diaza-*s*-indacen-8-yl)-pentyl]phenoxyacetamide (32)

Orange solid (55 mg, 30 % yield), mp 265°C. ^{1}H-NMR (500 MHz, DMSO-d_6): δ = 0.88 (t, 3H, 3´-CH_3), 1.42 (s, 2H, 2´CH_2-), 1.45-1.58 (m, 6H), 2.37 (s, 12H), 2.91 (m, 2H), 3.17 (dt, 2H), 3.80 (t, 2H), 4.54 (s, 2H), 6.19 (s, 2H), 7.06 und 8.03 (2d, 4H), 8.07 (t, 1H), 11.79 (s,1H), 13.43 (s, 1H). ^{13}C-NMR (125 MHz, DMSO-d_6): δ = 11.3 (s, 1C), 14.1 (t, 2C), 15.9 (s, 2C), 23.4 (s, 1C), 27.6 (s, 1C), 28.4 (s, 1C), 29.9.1 (s, 1C), 31.2 (s, 1C), 38.2 (s, 1C), 41.4 (s, 1C), 67.8 (s, 1C), 107.36 (s, 1C), 121.7 (s, 2C), 130.8 (s, 2C), 140.8 (s, 2C), 146.8 (s, 1C), 147.9 (s, 1C), 150.22 (s, 1C), 151.13 (s, 1C), 153.18 (s, 2C), 154.84 (s, 1C), 167.39 (s, 1C), 115.2, 122.2, 128.0, 128.7, 159.4 (5s, 6C). MS (ESI) (m/z): 658.3 $[M-H]^-$.

4-(1-Propyl-2,6-dioxo-2,3,6,7-tetrahydro-1*H*-purine-8-yl)-*N*-[10-(4,4-difluoro-1,3,5,7-tetramethyl-4-bora-3*a*,4*a*-diaza-*s*-indacen-8-yl)-decyl]phenoxyacetamide (33)

Orange solid (23 mg, 11 % yield), mp 262°C. ^{1}H-NMR (500 MHz, DMSO-d6): δ = 0.91 (t, 3H), 1.19-1.56 (m, 18H), 2.37 (s, 12H), 2.91 (m, 2H), 3.20 (t, 2H), 3.78 (t, 2H), 4.53 (s, 2H), 6.19 (s, 2H), 7.05 (dd, 2H), 8.03 (m, 3H), 11.79 (s, 1H), 13.43 (s, 1H). ^{13}C-NMR (125 MHz, DMSO-d_6): δ = 13.8 (s, 1C), 14.2 (s, 2C), 15.9 (s, 2C), 19.7 (s, 1C), 21.0 (s, 1C), 26.4 (s, 1C), 27.8 (s, 1C), 28.7 (s, 1C), 28.9 (s, 1C), 29.0 (s, 1C), 29.1 (s, 1C), 29.7 (s, 1C), 31.5 (s, 1C), 38.5 (s, 1C), 41.4 (s, 1C) 67.2 (s, 1C), 107.38 (s, 1C), 121.8 (s, 2C), 130.8 (s, 2C), 140.92 (s, 2C), 146.3 (s, 1C), 147.8 (s, 1C), 150.1 (s, 1C), 151.1 (s, 1C), 153.3 (s, 2C), 154.8 (s, 1C), 167.6 (s, 1C), 115.3, 122.2, 128.1, 159.3 (4s, 6C). MS (ESI) (m/z): 728.7 $[M-H]^-$.

Biological assays

Cell culture

Both nontransfected CHO-K1 cells and CHO-K1 cells stably expressing the human A_{2B}AR (CHO-hA_{2B} cells) were cultivated in Dulbecco's Modified Eagle Medium: Nutrient Mixture F-12 (DMEM/F12) supplemented with 10 % (v/v) fetal bovine serum (FCS), glutamine 2 mM, 100 U/ml penicillin and 100 µg/mL streptomycin. In contrast to CHO-K1 cells, CHO-hA_{2B} cells were cultured in the presence of 200 µg/mL G418.

Radioligand binding studies

Membrane preparations of CHO cells expressing human A_1AR, A_{2B}AR or A_3AR, mouse or rat A_{2B}ARs as well as brain cortical membrane preparations (A_1ARs) and rat brain striatal membrane preparations (A_{2A}ARs) were performed essentially as previously described.[55,56,63-65] Membrane preparations of human embryonic kidney (HEK) cells expressing human A_{2A}ARs were obtained from PerkinElmer (Product No.: RBHA2AM400UA).

Radioligand binding assays were performed as previously described.[55,56,63-65] Stock solutions of the compounds were prepared in dimethyl sulfoxide (DMSO). The final concentration in the assays was 2.5 %. Specific activities of the radioligands, their concentrations and incubation times (incubation at rt) were as follows: [^{3}H]CCPA: 42.6 Ci/mmol, 1 nM (rat and human A_1), 90 min; [^{3}H]MSX-2: 84 Ci/mmol, 1 nM (rat and human A_{2A}), incubation for 30 min; [^{3}H]PSB-11: 28 Ci/mmol, 1 nM (human A_3), 45 min; [^{3}H]PSB-603: 73 Ci/mmol, 0.3 nM (human, mouse, rat A_{2B}), 75 min. The nonradioactive precursors of [^{3}H]MSX-2[66] [^{3}H]PSB-603,[55] and [^{3}H]PSB-11[67] were synthesized in our laboratory. Membranes were pre-incubated for 10-15 min with 0.12 IU/mL of adenosine deaminase (ADA) in order to remove endogenous

adenosine. Nonspecific binding was determined in the presence of 10 μM 2-chloroadenosine (CADO) in A_1AR assays, 10 μM 9-chloro-2-(2-furyl)[1,2,4] triazolo[1,5-*c*]quinazolin-5-amine (CGS15943) in A_{2A}AR assays, 10 μM DPCPX in A_{2B}AR assays, and 100 μM (*R*)-N^6-phenylisopropyladenosine (*R*-PIA) in A_3AR assays. Incubation was terminated by rapid filtration using a Brandel 48-channel cell harvester (Brandel, Gaithersburg, MD) through Whatman GF/B glass fiber filters. Filters were rinsed three times with 2 mL each of ice-cold TRIS-HCl buffer (50 mM, pH 7.4) (containing 0.1 % bovine serum albumin (BSA) in A_{2B}AR assays) and incubated for 6-9 h with 2.5 mL of scintillation cocktail (Ready Safe™, Coulter) per well before radioactivity was counted in a liquid scintillation counter at an efficiency of 53 % (Tricarb 2900TR, Canberra Packard). Curves were determined using 6-7 different concentrations of test compounds spanning 3 orders of magnitude. At least three independent experiments were performed, each in duplicate (human receptors) or triplicate (rat receptors).

cAMP accumulation assays

The cAMP assays were performed as previously described.[56,68] In short, CHO cells stably overexpressing the human A_{2B}AR were pre-incubated with various dilutions of the antagonist for 1 h at 37°C and then stimulated with the agonist NECA (10 μM final concentration) for 5 min at 37°C. The reaction was stopped with hot (90 °C) lysis solution (4 mM EDTA, 0.01 % Triton X-100) in water. cAMP levels were quantified by a radioactive assay using [^{3}H]cAMP (Perkin-Elmer, Rodgau, Germany) and a cAMP binding protein prepared from bovine adrenal medulla[56,68]. The NECA (10 μM)-induced increase in cAMP concentration in the presence of the antagonist was expressed as percentage of the response to NECA in the absence of antagonist (% of control). Two to three independent experiments, each in duplicates, were performed.

Confocal imaging

CHO cells stably overexpressing the human A_{2B}AR were seeded at 5 x 10^4/mL and grown in sterile chambered coverslips (μ-slide 8 well, Cat.No: 80826, ibidi GmbH, Martinsried, Germany) to approx. 80 % confluency before imaging. Cells were incubated with **29** (100 nM) in the absence or presence (pre-incubation for 30 min) of **34** (100 nM) or DPCPX (1 μM), respectively, for 15 min. CHO wt cells used as controls were also treated with **29** (100 nM) under the same conditions.

Live cell imaging was performed using an inverted Nikon Eclipse A1 laser scanning confocal microscope (Nikon Corporation, Tokyo, Japan) equipped with a Plan-APO VC 60x oil immersion objective (NA 1.4, Nikon). Images were analyzed with NIS Element Advanced Research software 4.0 (Nikon Instrument, New York, USA). A 488 nm laser was used for excitation of **29** and emission was detected using a bandpass filter 515/30 (Nikon). All confocal images and their corresponding transmitted light images were taken using identical settings regarding laser power, detector offset and gain. Three independent experiments were performed.

Fluorescent ligand binding assay

CHO cells expressing the human A_{2B}AR were grown to 90 % confluency in 175 cm^2 cell culture flasks at 37°C and 5 % CO_2. The medium was discarded and the cells were pre-incubated with ADA (2 U/mL in DMEM-F12 medium) for 2 h at 37°C. Then the cells were washed with 15 mL of phosphate-buffered saline (PBS) and subsequently incubated with 5 mL of EDTA solution (5 mM in PBS) for 5 min to detach the cells. Medium (5 mL) was added to the flask, and the collected cells were centrifuged at 180 x g for 5 min. After removing the supernatant, the cell pellet was re-suspended in Hank´s Balanced Salt Solution (HBSS) supplemented with 2 U/mL of

ADA, and the cells were counted using a Fuchs-Rosenthal counting chamber. Cells were re-suspended in HBSS buffer (containing 2 U/mL ADA) and transferred into assay tubes (2.5×10^5 to 5×10^5 cells in 2 mL per vial). In preliminary fluorescent binding experiments the cells were incubated with different concentrations of the fluorescent ligand **29** for 1 h at 37°C. Nonspecific binding was determined in the presence of 100 nM **34**. For competition binding assays CHO-hA_{2B} cells were incubated with different concentrations of the standard A_{2B} antagonist **34** in the presence of 1 nM **29**. The final DMSO concentration did not exceed 1 %. After incubation with shaking for 60 min at 37ºC in the dark, the fluorescence of each sample was directly measured via flow cytometry (BD LSRII flow cytometer, BD Biosciences, San Jose, USA). Stained cell were analyzed using a blue laser (488 nm). Fluorescence was detected in a FITC channel using a 530/30 emission filter. Only single cell events were included in the analysis. At least 5000 events were recorded for each sample.

For measurements in a 96-well format cells were prepared as described above. For competition binding assays, the CHO-A_{2B} cell suspension was added into 96-well round-bottom plates at a density of 2.5 $x10^5$ cells per well. Cells were pre-treated with the antagonists for 30 min at 37°C and then incubated with **29 (**100 nM) for additional 20 min at 37°C. The A_{2B}-selective antagonist **34** (100 nM) was used to determine nonspecific binding. Fluorescence was measured using a guava easyCyte HT sampling flow cytometer (Merck Chemicals GmbH, Darmstadt, Germany). The fluorescent ligand **29** was excited with a blue laser (488 nm), and fluorescence was detected using the Green-B channel (525/30 nm). The mean fluorescence intensity, expressed in relative fluorescence units (RFU), was calculated for each sample. The fluorescence in the presence of the test compound was expressed as percentage of the fluorescence in the absence of test

compound (set as 100 %), and in the presence of 100 nM **34** (set as 0 %). Three to five independent experiments, each in duplicates, were performed.

Data analysis

Data were analyzed with GraphPad Prism, Version 6.0 (Graphpad, San Diego, CA, USA). For the calculation of K_i values by nonlinear regression analysis, the Cheng-Prusoff equation and the following K_D values were used: 0.21 nM (rat A_1AR) and 0.60 nM (human A_1AR) for [^{3}H]CCPA, 8.0 nM (rat A_{2A}AR) and 7.29 nM (human A_{2A}AR) for [^{3}H]MSX-2, 0.403 nM (human A_{2B}AR), 0.457 nM (rat A_{2B}AR) and 4.09 nM (mouse A_{2B}AR) for [^{3}H]PSB-603 and 4.9 nM (human A_3AR) for [^{3}H]PSB-11.[5,55,56,66,67,69,70]

Homology model

The X-ray structure of the human A_{2A}AR with an antagonist ZM241385 (PDB ID: 4EIY.pdb) was downloaded from the Research Collaboratory for Structural Bioinformatics (RCSB) Protein Data Bank[60] The structure was used as a template for generating a homology model of the human A_{2B}AR using Modeller9.[57] The sequence of the A_{2B}AR with the accession number of P29275 was retrieved from the UniProt sequence database (http:// http://www.uniprot.org/). The reasonable sequence similarity of 73.1 % and sequence identity of 58.3 % between the A_{2B}AR and the A_{2A}AR justified the choice of this structure as a template for the homology model. The sequences were aligned and visually interpreted for further improvement of the alignment. For each model, the variable target function method with conjugate gradients in Modeller was applied to optimize the model, followed by refinement using molecular dynamics with a simulated annealing method. Discrete Optimized Protein Energy (DOPE) score was utilized to

select the best model of A_{2B}AR from the 100 generated models.[71] The protonation of the selected model was done using the Protonate3D algorithm applying Molecular Operating Environment (MOE 2014.09) followed by minimization with a root mean square of 0.5 Å.[72] Ramachandran plot (Supplementary Figure S7) and PROSA II profile (Supplementary Figure S8) analysis confirmed the stereochemical quality and the sequence-structure compatibility of the model.[73,74]

Molecular Docking

The selected homology model of the human A_{2B}AR was applied for flexible ligand docking using AutoDock 4.2.[75] During the docking simulations, the ligands were fully flexible while the residues of the receptor were treated as rigid. Selected compounds were docked into the active site of the A_{2B}AR to predict the binding modes of the compounds. The atomic partial charges were added using AutoDockTools.[75,76] Fifty independent docking calculations using the *var*CPSO-ls algorithm from PSO@Autodock implemented in AutoDock4.2 were performed and terminated after 500,000 evaluation steps.[77] Parameters of *var*CPSO-ls algorithm, the cognitive and social coefficients c1 and c2 were set at 6.05 with 60 individual particles as swarm size. All the other parameters of the algorithm were set at their default values. Possible binding modes of the compounds were explored by visual inspection of the resulting docking poses.

ASSOCIATED CONTENT

Supporting Information

Absorption and emission spectra of **29**, representative 2D-dot-plots and histogram curves, ^{1}H-NMR, and ^{13}C-NMR of **29**, competition binding experiments of **32** at membrane preparations of recombinant CHO cells expressing rat or mouse A_{2B}ARs, pK_i values of **29** at the four AR

subtypes of different species, Ramachandran plot of the human A_{2B}AR model, sequence-structure compatibility of the human A_{2B}AR model, comparison of amino acid sequences of the human AR subtypes and molecular string formulae.

Homology Model

The atomic coordinates of the human A_{2B}AR homology model will be released upon article publication.

AUTHOR INFORMATION

Corresponding Authors

*Dr. Christa E. Müller

Pharmazeutisches Institut

Pharmazeutische Chemie I

An der Immenburg 4, D-53121 Bonn, Germany

Phone: +49-228-73-2301

Fax: +49-228-73-2567

E-mail: christa.mueller@uni-bonn.de

*Dr. Meryem Köse

Pharmazeutisches Institut

Pharmazeutische Chemie I

An der Immenburg 4, D-53121 Bonn, Germany

Phone: +49-228-73-7860

Fax: +49-228-73-2567

E-mail: mkoese@uni-bonn.de

ACKNOWLEDGMENTS

We thank Marion Schneider for LCMS analyses, Sabine Terhart-Krabbe and Annette Reiner for NMR spectra, and Katharina Sylvester for performing biological assays. We are grateful to Prof. Dr. Markus Sauer and Dr. Ralf Brune for providing the infrastructure and guidance to determine fluorescent quantum yields. Prof. Dr. Michael Wiese, Katja Silbermann and Dieter Baumert are gratefully acknowledged for allowing us to use the flow cytometer in their department and for providing initial guidance. This study was partly supported by Polish National Science Center funding, project DEC-2012/04/M/NZ4/00219. We are also grateful for support by the COST Action CM1207 and by the Deutscher Akademischer Austauschdienst (PPP project No. 56269592).

ABBREVIATIONS USED

AcOH, acetic acid; AR, adenosine receptor; A_1AR, A_1 adenosine receptor; A_{2A}AR, A_{2A} adenosine receptor; A_{2B}AR, A_{2B} adenosine receptor; A_3AR, A_3 adenosine receptor; Alexa-Flour-488, 3,6-diamino-9-[2,4(or 2,5)-dicarboxyphenyl]-4,5-disulfoxanthylium; Alexa-Flour-532, 5-(4-carboxyphenyl)-1,2,3,7,8,9-hexahydro-2,3,3,7,7,8-hexamethyl-10,12-disulfo-pyrano[3,2-*f*:5,6-*f'*] diindol-11-ium; BODIPY, boron dipyrromethene; ADA, adenosine deaminase; BSA, bovine serum albumin; CADO, 2-chloroadenosine; CCPA, 2-chloro-N^6-cyclopentyladenosine;

CGS15943, 9-chloro-2-(2-furanyl)[1,2,4]triazolo[1,5-*c*]quinazolin-5-amine; CGS21680, 4-[2-[[6-amino-9-(N-ethyl-β-D-ribofuranuronamidosyl)-9*H*-purin-2-yl]amino]ethyl]benzene-propanoic acid; CHO, Chinese hamster ovary cells; DIPEA, diisopropylethylamine; DMAP, 4-(dimethylamino)-pyridine; DCM, dichloromethane; DIPEA, *N,N*-diisopropylethylamine; DMF, dimethylformamide; DMSO, dimethyl sulfoxide; DPCPX, 8-cyclopentyl-1,3-dipropylxanthine; EDMA, ethyldimethylamine; EDTA, ethylenediaminetetraacetic acid; FACS, fluorescence-activated cell sorting; FCS, fetal bovine serum; FCS, fluorescence correlation spectroscopy; FITC, fluorescein isothiocyanate; FP, fluorescence polarization; FRAP, fluorescence recovery after photobleaching; GPCR, G protein-coupled receptor; h, human; HBSS, Hank´s balanced salt solution; HCTU, 2-(6-chloro-1*H*-benzotriazol-1-yl)-1,1,3,3-tetramethyluronium hexafluorophosphate; HEK cells, human embryonic kidney cells; HMDS, hexamethyldisilazane; MeOH, methanol; NECA, 5'-N-ethylcarboxamido-adenosine; PET, positron emission tomography; PBS, phosphate-buffered saline; PSB-0788, 8-(4-(4-(4-chlorobenzyl)piperazine-1-sulfonyl)phenyl)-1-propylxanthine; PSB-601, 8-[4-(4-benzylpiperazide-1-sulfonyl)phenyl]-1-propylxanthine; PSB-603, 8-[4-[4-(4-chlorophenzyl)piperazide-1-sulfonyl)phenyl]]-1-propylxanthine; PyBOP, benzotriazol-1-yl-oxytripyrrolidinophosphonium hexafluorophosphate; r, rat; RCSB, research collaboratory for structural bioinformatics; TLC, thin layer chromatography; TM, transmembrane domain; XAC, 8-[4-[[[[(2-aminoethyl)amino]carbonyl]methyl]oxy]phenyl]-l,3-dipropylxanthine; ZM-241385, 4-(2-[7-amino-2-(2-furyl)-[1,2,4]triazolo-[2,3-*a*][1,3,5]triazin-5-ylamino]ethyl)-phenol

REFERENCES

1. Fredholm, B. B.; IJzerman A. P.; Jacobson, K. A.; Linden, J.; Müller, C. E. International union of basic and clinical pharmacology. LXXXI. Nomenclature and classification of adenosine receptors-an update. *Pharmacol. Rev.* **2011,** *63*, 1-34.

2. Elzein, E.; Zablocki, J. A_1 adenosine receptor agonists and their potential therapeutic applications. *Expert Opin. Invest. Drugs* **2008,** *17*, 1901-1910.

3. Hasko, G.; Linden, J.; Cronstein, B.; Pacher, P. Adenosine receptors: therapeutic aspects for inflammatory and immune diseases. *Nat. Rev. Drug Discovery* **2008,** *7*, 759-770.

4. Kolachala, V. L.; Vijay-Kumar, M.; Dalmasso, G.; Yang, D.; Linden, J.; Wang, L.; Gewirtz, A.; Ravid, K.; Merlin, D.; Sitaraman, S. V. A_{2B} adenosine receptor gene deletion attenuates murine colitis. *Gastroenterology* **2008,** *135*, 861-870.

5. El-Tayeb, A.; Michael, S.; Abdelrahman, A.; Behrenswerth, A.; Gollos, S.; Nieber, K.; Müller, C. E. Development of polar adenosine A_{2A} receptor agonists for inflammatory bowel disease: synergism with A_{2B} antagonists. *Med. Chem. Lett.* **2011,** *2*, 890-895.

6. Field, J. J.; Nathan, D. G.; Linden, J. The role of adenosine signaling in sickle cell therapeutics. *Hematol. Oncol. Clin. North Am.* **2008,** *28*, 287-299.

7. Wei, Q.; Costanzi, S.; Balasubramanian, R.; Gao, Z. G.; Jacobson, K. A. A_{2B} adenosine receptor blockade inhibits growth of prostate cancer cells. *Purinergic Signal.* **2013**, *9*, 271-280.

8. Allard, D.; Turcotte, M.; Stagg, J. Targeting A2 adenosine receptors in cancer. I*mmunol. Cell Biol.* **2017**, *95*, 333-339.

9. Fernandez-Gallardo, M.; González-Ramírez, R.; Sandoval, A.; Felix, R.; Monjaraz, E. Adenosine stimulate proliferation and migration in triple negative breast cancer cells. *PLoS One* **2016**, *11*, e0167445.

10. Hinz, S.; Navarro, G.; Borroto-Escuela, D.; Seibt, B. F.; Ammon, Y.-C.; de Filippo, E.; Danish, A.; Lacher, S. K.; Červinková, B.; Rafehi, M.; Fuxe, K.; Schiedel, A. C.; Franco, R.; Müller, C. E. Adenosine A_{2A} receptor ligand recognition and signaling is blocked by A_{2B} receptors. *Oncotarget*, **2018**, *9*, 13593-13611.

11. Kecskes, M.; Kumar, T. S.; Yoo, L.; Gao, Z. G.; Jacobson, K. A. Novel Alexa Fluor-488 labeled antagonist of the A_{2A} adenosine receptor: application to a fluorescence polarization-based receptor binding assay. *Biochem. Pharmacol.* **2010,** *80*, 506-511.

12. Middleton, R. J.; Briddon, S. J.; Cordeaux, Y.; Yates, A. S.; Dale, C. L.; George, M. W.; Baker, J. G.; Hill, S. J.; Kellam, B. New fluorescent adenosine A_1-receptor agonists that allow quantification of ligand-receptor interactions in microdomains of single living cells. *J. Med. Chem.* **2007**, *50*, 782-793.

13. Briddon, S. J.; Middleton, R. J.; Cordeaux, Y.; Flavin, F. M.; Weinstein, J. A.; George, M. W.; Kellam, B.; Hill, S. J. Quantitative analysis of the formation and diffusion of A_1-adenosine receptor-antagonist complexes in single living cells. *Proc. Natl. Acad. Sci.* **2004**, *101*, 4673-4678.

14. Briddon, S. J.; Middleton, R. J.; Yates, A. S.; George, M. W.; Kellam, B.; Hill, S. J. Application of fluorescence correlation spectroscopy to the measurement of agonist binding to a G-protein coupled receptor at the single cell level. *Faraday Discuss.* **2004,** *126*, 197-207; discussion 245-254.

15. Fernández-Dueñas, V.; Gómez-Soler, M.; Jacobson, K. A.; Kumar, S. T.; Fuxe, K.; Borroto-Escuela, D. O.; Ciruela, F. Molecular determinants of $A_{2A}R$-D_2R allosterism: role of the intracellular loop 3 of the D_2R. *J. Neurochem*. **2012**, *123*, 373-384.

16. Fernandez-Duenas, V.; Gomez-Soler, M.; Morato, X.; Nunez, F.; Das, A.; Kumar, T. S.; Jauma, S.; Jacobson, K. A.; Ciruela, F. Dopamine D_2 receptor-mediated modulation of adenosine A_{2A} receptor agonist binding within the $A_{2A}R/D_2R$ oligomer framework. *Neurochem. Int.* **2013,** *63*, 42-46.

17. Kozma, E.; Kumar, T. S.; Federico, S.; Phan, K.; Balasubramanian, R.; Gao, Z. G.; Paoletta, S.; Moro, S.; Spalluto, G.; Jacobson, K. A. Novel fluorescent antagonist as a molecular probe in A_3 adenosine receptor binding assays using flow cytometry. *Biochem. Pharmacol.* **2012,** *83*, 1552-1561.

18. Lalo, U.; Allsopp, R. C.; Mahaut-Smith, M. P.; Evans, R. J. P2X1 receptor mobility and trafficking; regulation by receptor insertion and activation. *J. Neurochem.* **2010,** *113*, 1177-1187.

19. Kumar, T. S.; Mishra, S.; Deflorian, F.; Yoo, L. S.; Phan, K.; Kecskes, M.; Szabo, A.; Shinkre, B.; Gao, Z. G.; Trenkle, W.; Jacobson, K. A. Molecular probes for the A_{2A} adenosine receptor based on a pyrazolo[4,3-*e*][1,2,4]triazolo[1,5-*c*]pyrimidin-5-amine scaffold. *Bioorg. Med. Chem. Lett.* **2011,** *21*, 2740-2745.

20. Stoddart, L. A.; Vernall, A. J.; Denman, J. L.; Briddon, S. J.; Kellam, B.; Hill, S. J. Fragment screening at adenosine-A_3 receptors in living cells using a fluorescence-based binding assay. *Chem. Biol.* **2012,** *19*, 1105-1115.

21. Macchia, M.; Salvetti, F.; Bertini, S.; Di Bussolo, V.; Gattuso, L.; Gesi, M.; Hamdan, M.; Klotz, K. N.; Laragione, T.; Lucacchini, A.; Minutolo, F.; Nencetti, S.; Papi, C.; Tuscano, D.; Martini, C. 7-Nitrobenzofurazan (NBD) derivatives of 5'-N-ethylcarboxamidoadenosine (NECA) as new fluorescent probes for human A_3 adenosine receptors. *Bioorg. Med. Chem. Lett.* **2001,** *11*, 3023-3026.

22. Macchia, M.; Salvetti, F.; Barontini, S.; Calvani, F.; Gesi, M.; Hamdan, M.; Lucacchini, A.; Pellegrini, A.; Soldani, P.; Martini, C. Fluorescent probes for adenosine receptors: synthesis and biology of N^6-dansylaminoalkyl-substituted NECA derivatives. *Bioorg. Med. Chem. Lett.* **1998,** *8*, 3223-3228.

23. May, L. T.; Briddon, S. J.; Hill, S. J. Antagonist selective modulation of adenosine A_1 and A_3 receptor pharmacology by the food dye Brilliant Black BN: evidence for allosteric interactions. *Mol. Pharmacol.* **2010,** *77*, 678-686.

24. Das, A.; Sanjayan, G. J.; Kecskes, M.; Yoo, L.; Gao, Z. G.; Jacobson, K. A. Nucleoside conjugates of quantum dots for characterization of G protein-coupled receptors: strategies for immobilizing A_{2A} adenosine receptor agonists. *J. Nanobiotechnol.* **2010**, *8*, 11.

25. Kecskes, A.; Tosh, D. K.; Wei, Q.; Gao, Z. G.; Jacobson, K. A. GPCR ligand dendrimer (GLiDe) conjugates: adenosine receptor interactions of a series of multivalent xanthine antagonists. *Bioconjugate Chem.* **2011,** *22*, 1115-1127.

26. Tosh, D. K.; Chinn, M.; Ivanov, A. A.; Klutz, A. M.; Gao, Z. G.; Jacobson, K. A. Functionalized congeners of A_3 adenosine receptor-selective nucleosides containing a bicyclo[3.1.0]hexane ring system. *J. Med. Chem*. **2009**, *52*, 7580-7592.

27. Tosh, D. K.; Chinn, M.; Yoo, L. S.; Kang, D. W.; Luecke, H.; Gao, Z. G.; Jacobson, K. A. 2-Dilkynyl derivatives of (N)-methanocarba nucleosides: 'clickable' A_3 adenosine receptor-selective agonists. *Bioorg. Med. Chem.* **2010,** *18*, 508-517.

28. Tosh, D. K.; Yoo, L. S.; Chinn, M.; Hong, K.; Kilbey, S. M., 2nd; Barrett, M. O.; Fricks, I. P.; Harden, T. K.; Gao, Z. G.; Jacobson, K. A. Polyamidoamine (PAMAM) dendrimer conjugates of "clickable" agonists of the A_3 adenosine receptor and coactivation of the $P2Y_{14}$ receptor by a tethered nucleotide. *Bioconjugate Chem.* **2010,** *21*, 372-384.

29. Tosh, D. K.; Deflorian, F.; Phan, K.; Gao, Z. G.; Wan, T. C.; Gizewski, E.; Auchampach, J. A.; Jacobson, K. A. Structure-guided design of A_3 adenosine receptor-selective nucleosides: combination of 2-arylethynyl and bicyclo[3.1.0]hexane substitutions. *J. Med. Chem*. **2012**, *55*, 4847-4860.

30. Vernall, A. J.; Stoddart, L. A.; Briddon, S. J.; Hill, S. J.; Kellam, B. Highly potent and selective fluorescent antagonists of the human adenosine A_3 receptor based on the 1,2,4-triazolo[4,3-*a*]quinoxalin-1-one scaffold. *J. Med. Chem.* **2012,** *55*, 1771-1782.

31. Brand, F.; Klutz, A. M.; Jacobson, K. A.; Fredholm, B. B.; Schulte, G. Adenosine A_{2A} receptor dynamics studied with the novel fluorescent agonist Alexa488-APEC. *Eur. J. Pharmacol.* **2008,** *590*, 36-42.

32. McCabe, R. T.; Skolnick, P.; Jacobson, K. A. 2-[2-[4-[2-[2-[1,3-Dihydro-1,1-bis(4-hydroxyphenyl)-3-oxo-5-isobenzofuranthioureidyl]ethylaminocarbonyl]ethyl]phenyl] ethylamino]-5′-N-ethylcarboxamidoadenosine (FITC-APEC): a fluorescent ligand for A_{2A}-adenosine receptors. *J. Fluoresc.* **1992,** *2*, 217-223.

33. Jacobson, K. A.; Ukena, D.; Padgett, W.; Kirk, K. L.; Daly, J. W. Molecular probes for extracellular adenosine receptors. *Biochem. Pharmacol.* **1987**, *36*, 1697-1707.

34. Baker, J. G.; Middleton, R.; Adams, L.; May, L. T.; Briddon, S. J.; Kellam, B.; Hill, S. J. Influence of fluorophore and linker composition on the pharmacology of fluorescent adenosine A_1 receptor ligands. *Br. J. Pharmacol.* **2010,** *159*, 772-786.

35. Dreyfuss, G.; Schwartz, K.; Blout, E. R.; Barrio, J. R.; Liu, F. T.; Leonard, N. J. Fluorescent photoaffinity labeling: adenosine 3',5'-cyclic monophosphate receptor sites. *Proc. Natl. Acad. Sci.* **1978,** *75*, 1199-1203.

36. Vernall, A. J.; Stoddart, L. A.; Briddon, S. J.; Ng, H. W.; Laughton, C. A.; Doughty, S. W.; Hill, S. J.; Kellam, B. Conversion of a non-selective adenosine receptor antagonist into A_3-selective high affinity fluorescent probes using peptide-based linkers. *Org. Biomol. Chem.* **2013,** *11*, 5673-5682.

37. Fernández-Dueñas, V.; Taura, J. J.; Cottet, M.; Gómez-Soler, M.; López-Cano, M.; Ledent, C.; Watanabe, M.; Trinquet, E.; Pin, J. P.; Luján, R.; Durroux, T.; Ciruela, F. Untangling dopamine-adenosine receptor-receptor assembly in experimental parkinsonism in rats. *Dis. Model. Mech.* **2015**, *8*, 57-63.

38. Kuder, K.; Kieć-Kononowicz, K. Fluorescent GPCR ligands as new tools in pharmacology. *Curr. Med. Chem.* **2008**, *15*, 2132-2143.

39. Kozma, E.; Suresh Jayasekara, P.; Squarcialupi, L.; Paoletta, S.; Moro, S.; Federico, S.; Spalluto, G.; Jacobson, K. A. Fluorescent ligands for adenosine receptors. *Bioorg. Med. Chem. Lett.* **2013,** *23*, 26-36.

40. Middleton, R. J.; Kellam, B. Fluorophore-tagged GPCR ligands. *Curr. Opin. Chem. Biol.* **2005**, *9*, 517-525.

41. Cordeaux, Y.; Briddon, S. J.; Alexander, S. P.; Kellam, B.; Hill, S. J. Agonist-occupied A_3 adenosine receptors exist within heterogeneous complexes in membrane microdomains of individual living cells. *FASEB J.* **2008**, *22*, 850-860.

42. Dale, C. L. H.; Hill, S. J.; Kellam, B. New potent, short-linker BODIPY-630/650 labelled fluorescent adenosine receptor agonists. *MedChemComm* **2012,** *3*, 333-338.

43. Wysocki, L. M.; Lavis, L. D. Advances in the chemistry of small molecule fluorescent probes. *Curr. Opin. Chem. Biol.* **2011,** 15, 752-759.

44. Treibs, A.; Kreuzer, F.-H. Difluorboryl-Komplexe von di- und tripyrrylmethenen. *Liebigs Ann.* **1968**, *718*, 208-223.

45. Loudet, A.; Burgess, K. BODIPY dyes and their derivatives: syntheses and spectroscopic properties. *Chem. Rev.* **2007**, *107*, 4891-4932.

46. Karolin, J.; Johansson, L. B. A.; Strandberg, L.; Ny, T. Fluorescence and absorption spectroscopic properties of dipyrrometheneboron difluoride (BODIPY) derivatives in liquids, lipid membranes, and proteins. *J. Am. Chem. Soc.* **1994,** *116*, 7801-7806.

47. Johnson, I. D.; Kang, H. C.; Haugland, R. P. Fluorescent membrane probes incorporating dipyrrometheneboron difluoride fluorophores. *Anal. Biochem.* **1991,** *198*, 228-237.

48. Gollos, S., Heisig, S., Freudenthal, S. J., El-Tayeb, A., Iqbal, J., Müller, C. E. Synthesis of BODIPY derivatives substituted with various bioconjugatable linker groups: a construction kit for fluorescent labeling of receptor ligands. *J. Fluoresc*. **2014**, *24*, 213-230.

49. Müller, C. E.; , Jacobson, K. A. Xanthines as adenosine receptor antagonists. *Handb. Exp. Pharmacol.* **2011**, *200*, 151-199.

50. Thimm, D.; Schiedel, A. C.; Sherbiny, F. F.; Hinz, S.; Hochheiser, K.; Bertarelli, D. C.; Maass, A.; Müller, C. E. Ligand-specific binding and activation of the human adenosine A_{2B} receptor. *Biochemistry* **2013**, *52*, 726-40.

51. Müller, C. E.; Sandoval-Ramirez, J. A versatile synthesis of xanthines with variable substituents in the 1-, 3-, 7-, and 8- positions. *Synthesis* **1995**, 1295-1299.

52. Hayallah, A. M.; Sandoval-Ramirez, J.; Reith, U.; Schobert, U.; Preiss, B.; Schumacher, B.; Daly, J. W.; Müller, C. E. 1,8-disubstituted xanthine derivatives: synthesis of potent A_{2B}-selective adenosine receptor antagonists. *J. Med. Chem.* **2002**, *45*, 1500-1510.

53. Müller, C. E. Synthesis of 3-substituted 6-aminouracils. *Tetrahedron Lett.* **1991**, *32*, 6539-6540.

54. Müller, C. E. General synthesis and properties of 1-monosubstituted xanthines. *Synthesis* **1993**, *1*, 125-128.

55. Borrmann, T.; Hinz, S.; Bertarelli, D. C.; Li, W.; Florin, N. C.; Scheiff, A. B.; Müller, C. E. 1-alkyl-8-(piperazine-1-sulfonyl)phenylxanthines: development and characterization of adenosine A_{2B} receptor antagonists and a new radioligand with subnanomolar affinity and subtype specificity. *J. Med. Chem.* **2009**, *52,* 3994-4006.

56. Alnouri, M. W.; Jepards, S.; Casari, A.; Schiedel, A. C.; Hinz, S.; Müller, C. E. Selectivity is species-dependent: characterization of standard agonists and antagonists at human, rat, and mouse adenosine receptors. *Purinergic Signalling* **2015,** *11*, 389-407.

57. Sali, A.; Blundell, T. L. Comparative protein modelling by satisfaction of spatial restraints. *J. Mol. Biol.* **1993**, *234*, 779-815.

58. Evstigneev, M. P. Hetero-association of aromatic molecules in aqueous solution. *Int. Rev. Phys. Chem.* **2014**, *33*, 229-273.

59. Jaakola, V.-P.; Griffith, M. T.; Hanson, M. A.; Cherezov, V.; Chien, E. Y. T.; Lane, J. R.; IJzerman, A. P.; Stevens, R. C. The 2.6 Å crystal structure of a human A_{2A} adenosine receptor bound to an antagonist. *Science* **2008**, *322*, 1211-1217.

60. Liu, W.; Chun, E.; Thompson, A. A.; Chubukov, P.; Xu, F.; Katritch, V.; Han, G. W.; Roth, C. B.; Heitman, L. H.; IJzerman, A. P.; Cherezov, V.; Stevens, R. C. Structural basis for allosteric regulation of GPCRs by sodium ions. *Science* **2012**, *337*, 232-236.

61. Doré, A. S.; Robertson, N.; Errey, J. C.; Ng, I.; Hollenstein, K.; Tehan, B.; Hurrell, E.; Bennett, K.; Congreve, M.; Magnani, F.; Tate, C. G.; Weir, M.; Marshall, F. H. Structure of the

adenosine A_{2A} receptor in complex with ZM241385 and the xanthines XAC and caffeine. *Structure* **2011**, *19*, 1283-1293.

62. Cheng, R. K. Y.; Segala, E.; Robertson, N.; Deflorian, F.; Doré, A. S.; Errey, J. C.; Fiez-Vandal, C.; Marshall, F. H.; Cooke, R. M. Structures of human A_1 and A_{2A} adenosine receptors with xanthines reveal determinants of selectivity. *Structure* **2017**, *25*, 1275-1285.e4.

63. Klotz, K. N.; Hessling, J.; Hegler, J.; Owman, C.; Kull, B.; Fredholm, B. B.; Lohse, M. J. Comparative pharmacology of human adenosine receptor subtypes - characterization of stably transfected receptors in CHO cells. *Arch. Pharmacol.* **1998**, *357*, 1-9.

64. Weyler, S.; Fülle, F.; Diekmann, M.; Schumacher, B.; Hinz, S.; Klotz, K. N.; Müller, C. E. Improving potency, selectivity, and water solubility of adenosine A_1 receptor antagonists: xanthines modified at position 3 and related pyrimido[1,2,3-*cd*]purinediones. *ChemMedChem* **2006**, *1*, 891-902.

65. Drabczyńska, A.; Müller, C. E.; Karolak-Wojciechowska, J.; Schumacher, B.; Schiedel, A.; Yuzlenko, O.; Kieć-Kononowicz, K. N^9-benzyl-substituted 1,3-dimethyl- and 1,3-dipropyl-pyrimido[2,1-*f*]purinediones: synthesis and structure-activity relationships at adenosine A_1 and A_{2A} receptors. *Bioorg. Med. Chem.* **2007**, *15*, 5003-5017.

66. Müller, C. E.; Maurinsh, J.; Sauer, S. Binding of [^{3}H]MSX-2 (3-(3-hydroxypropyl)-7-methyl-8-(m-methoxystyryl)-1-propargylxanthine) to rat striatal membranes-a new, selective antagonist radioligand for A_{2A} adenosine receptors. *Eur. J. Pharm. Sci.* **2000**, *10*, 259–265.

67. Müller, C.E.; Diekmann, M.; Thorand, M.; Ozola, V. [^{3}H]8-Ethyl-4-methyl-2-phenyl-(8*R*)-4,5,7,8-tetrahydro-1*H*-imidazo[2,1-*i*]purin-5-one ([^{3}H]PSB-11), a novel high-affinity antagonist radioligand for human A_3 adenosine receptors. *Bioorg. Med. Chem. Lett.* **2002**, *12*, 501– 503.

68. Nordstedt, C.; Fredholm, B. B. A modification of a proteinbinding method for rapid quantification of cAMP in cell-culture supernatants and body fluid. *Anal. Biochem*. **1990**, *189*, 231–234.

69. El-Tayeb, A.; Iqbal, J.; Behrenswerth, A.; Romio, M.; Schneider, M.; Zimmermann, H.; Schrader, J.; Müller, C. E. Nucleoside-5'-monophosphates as prodrugs of adenosine A_{2A} receptor agonists activated by ecto-5'-nucleotidase. *J. Med. Chem.* **2009**, *52*, 7669-7677.

70. Bruns, R. F.; Lu, G. H.; Pugsley, T. A. Characterization of the A_2 adenosine receptor labeled by [^{3}H]NECA in rat striatal membranes. *Mol. Pharmacol.* **1986**, *29*, 331-346.

71. Shen, M. Y.; Sali, A. Statistical potential for assessment and prediction of protein structures. *Protein Sci.* **2006,** *15*, 2507-2524.

72. *Molecular operating environment (MOE 2014.09); chemical computing group*. Montreal, Quebec, Canada, 2014.

73. Lovell, S. C.; Davis, I. W.; Arendall, W. B., 3rd; de Bakker, P. I.; Word, J. M.; Prisant, M. G.; Richardson, J. S.; Richardson, D. C. Structure validation by Calpha geometry: phi, psi and Cbeta deviation. *Proteins* **2003**, *50*, 437-450.

74. Wiederstein, M.; Sippl, M. J. ProSA-web: interactive web service for the recognition of errors in three-dimensional structures of proteins. *Nucleic Acids Res.* **2007,** *35*, W407-410.

75. Morris, G.; Huey, R.; Lindstrom, W.; Sanner, M.; Belew, R.; Goodsell, S.; Olson, J. J. AutoDock4 and AutoDockTools4: automated docking with selective receptor flexibility. *J. Comput. Chem.* **2009**, *30*, 2785–2791.

76. Sanner, M. Python: a programming language for software integration and development. *J. Mol. Graph. Model.* **1999**, *17*, 57–61.

77. Namasivayam, V.; Günther, R. PSO@autodock: A fast flexible molecular docking program based on swarm intelligence. *Chem. Biol. Drug Des.* **2007**, *70*, 475-484.

TOC graphic

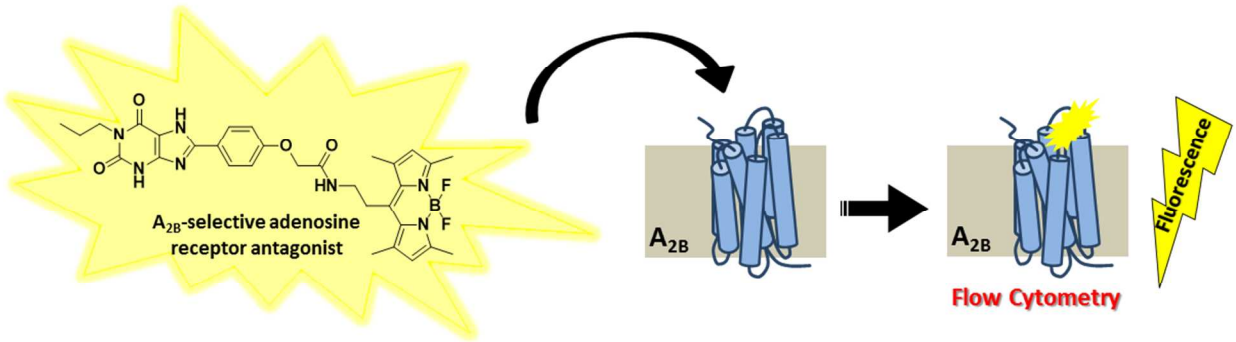
A2B-selective adenosine receptor antagonist
A2B
A2B
Flow Cytometry
Fluorescence

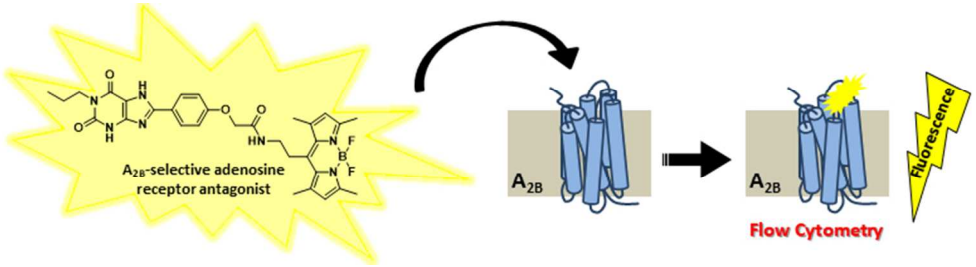

210x55mm (96 x 96 DPI)